AD_____

Award Number: W81XWH-07-1-0428

TITLE: Nanotechnology-Enabled Optical Molecular Imaging
of Breast Cancer

PRINCIPAL INVESTIGATOR: Rebekah Drezek, Ph.D.

CONTRACTING ORGANIZATION: Rice University
                                     Houston, TX 77005

REPORT DATE: July 2010

TYPE OF REPORT: Annual

PREPARED FOR: U.S. Army Medical Research and Material Command
                     Fort Detrick, Maryland 21702-5012

DISTRIBUTION STATEMENT:

      X ☐ Approved for public release; distribution unlimited

REPORT DOCUMENTATION PAGE

1. REPORT DATE *(DD-MM-YYYY)* 01-07-2010	**2. REPORT TYPE** Annual	**3. DATES COVERED** *(From - To)* 15 JUN 2009 - 14 JUN 2010

4. TITLE AND SUBTITLE Nanotechnology-Enabled Optical Molecular Imaging of Breast Cancer	**5a. CONTRACT NUMBER**
	5b. GRANT NUMBER W81XWH-07-1-0428
	5c. PROGRAM ELEMENT NUMBER
6. AUTHOR(S) Rebekah Drezek, Ph.D. drezek@rice.edu	**5d. PROJECT NUMBER**
	5e. TASK NUMBER
	5f. WORK UNIT NUMBER

7. PERFORMING ORGANIZATION NAME(S) AND ADDRESS(ES) Rice University PO Box 1892 Houston, TX 77251-1892	**8. PERFORMING ORGANIZATION REPORT NUMBER**

9. SPONSORING / MONITORING AGENCY NAME(S) AND ADDRESS(ES) DOD CDMRP in Breast Cancer U.S. Army Medical Research and Material Fort Detrick, Maryland 21702-5012	**10. SPONSOR/MONITOR'S ACRONYM(S)** DOD CDMRP in Breast Cancer
	11. SPONSOR/MONITOR'S REPORT NUMBER(S)

12. DISTRIBUTION / AVAILABILITY STATEMENT
Approved for public release; distribution unlimited

13. SUPPLEMENTARY NOTES

14. ABSTRACT
This project focuses on development of nanotechnology-enabled optical molecular imaging technologies for applications in both breast cancer diagnosis and monitoring therapeutic response. The project consists of two major efforts: (1) optical instrumentation technology development and (2) development of complementary engineered nanomaterials for use in conjunction with the instrumentation created to provide molecular specificity. A particularly significant effort is underway to develop a needle-compatible fiber optic probe to enable in vivo imaging of tumors with micron resolution in order to provide a new microscopic, high resolution imaging modality to complement the low resolution, macroscopic imaging modalities already in common clinical use. An initial journal publication describing the single fiber needle-compatible microendoscope was recently accepted and a provisional patent application was filed on this technology during the most recent reporting period.

15. SUBJECT TERMS
nanotechnology, molecular imaging, optical imaging

16. SECURITY CLASSIFICATION OF:			**17. LIMITATION OF ABSTRACT**	**18. NUMBER OF PAGES**	**19a. NAME OF RESPONSIBLE PERSON** Dr. Rebekah Drezek
a. REPORT U	**b. ABSTRACT** U	**c. THIS PAGE** U	UU	55	**19b. TELEPHONE NUMBER** *(include area code)* 713-348-3011

Table of Contents

Introduction

There is a critical need to develop new imaging technologies which bridge the gap between our rapidly developing fundamental molecular understanding of breast carcinogenesis and our ability to rationally harness this understanding to develop more effective diagnostic and treatment strategies. Bridging that gap requires developing new tools which can rapidly detect, diagnose, and at times, intervene in the disease process based on recognition of specific molecular signatures of breast cancer *in vivo*. In this project, we focus on the development of photonics-based imaging technologies (SOW, Project 1 and Project 2) and complementary nanoscale molecular-targeted imaging agents for detection and monitoring applications (SOW, Project 3) in order to provide a new approach to molecular imaging of breast cancer. Medical imaging plays a prominent role in all aspects of the screening, detection, and management of breast cancer today. A variety of imaging methods including screening and diagnostic x-ray mammography and resonance imaging (MRI) are currently used to evaluate and monitor breast lesions. Although existing imaging technologies provide a useful approach to delineating the extent of tumors, these methods offer only low resolution, non-specific issues of tissue and cannot provide a detailed picture of the molecular profile of a tumor. In addition, techniques such as x-ray imaging and MRI are not able to detect small early cancers or pre-cancerous breast lesions and are difficult to use in settings such as the operating room where near real-time dynamic images are required. Thus, there is a substantial clinical need for novel imaging methods for the detection and monitoring of breast cancers which offer improved sensitivity, specificity, portability, and cost-effectiveness. In this project we develop portable optical technologies which promise high resolution, noninvasive functional imaging of tissue at competitive costs. Optical approaches can detect a broad range of morphological, biochemical, and architectural tissue features directly relevant to characterizing breast lesions including sub-cellular physical parameters such as nuclear size and nuclear to cytoplasm (N/C) ratios and biochemical indicators such as hemoglobin concentration, metabolic rate, and collagen cross-linking levels. To make these technologies even more powerful we are expanding the current capabilities of photonics-based imaging approaches with the additional capacity to quantitatively and dynamically detect molecular markers of breast cancer *in vivo* without tissue removal or directly after removal in a surgical environment (SOW, Project 3). Developing the optical molecular imaging tools and agents for breast cancer which will allow us to accomplish this goal is the focus of this project. We have now completed three years of effort on this project. The SOW has been modified once to reflect revised goals and to include tissue studies rather than stopping at the cell based studies originally proposed. The projects are progressing on schedule, and a provisional patent application was submitted during the reporting year for the new fiber bundle microendoscopes we have developed through the Era of Hope award.

PROGRESS REPORT BODY

The body of the progress report is contained in this section. In cases where published papers provide more details on our methods, these materials are referred to within the report, and the papers appear as pdfs appended to the end of the report. Some of the text in the sections below is derived from those papers and from those which have not yet appeared in print. In general, we have kept the sections of the report focusing on already published work shorter while the portions reporting on work not yet published in the literature are somewhat more detailed. The numbering of projects and tasks discussed in the report corresponds to the numbers used in our currently approved Statement of Work.

To briefly summarize the overall structure of the current SOW, this Era of Hope award is comprised of three active projects of which the first project involves the most substantial effort. Two of the projects focus on instrumentation development, and the third project focuses on nanoparticle-based imaging agents. The instrumentation projects include a microscopic (high resolution, small field of view) imaging effort and a macroscopic imaging (low resolution, large field of view) effort. The microscopic imaging effort is intended to develop new ways of visualizing breast tissue at high (cellular to sub-cellular) resolution without having to remove tissue from the body or even necessarily stain/label the tissue in any kind of way though labeling is needed for some molecular imaging applications. The systems being built in Project 1 provide real time, video rate imaging. The systems can detect optical signals based on either reflectance (scatter) contrast or fluorescence (emission) contrast. This contrast can derive from intrinsic features of the tissue or may be generated through the use of exogenous imaging agents. Because the field of view at high resolution is limited, placement of the microscopic systems (where to image at high resolution) can be guided by the use of low resolution, macroscopic optical imaging systems. Because there is generally a need for tissue level surveillance to guide cell level imaging, we have developed a macroscopic imaging system (Project 2) to complement the microscopic imaging systems (Project 1). This system will be needed for tumor margin evaluation. The macroscopic imaging system, like the microscopic ones, can be used in either reflectance or fluorescence mode and also incorporates polarization. Because it combines multiple optical modalities, it is termed a multi-modal optical (MOI) imaging system in this report. It is important to be aware that while both the microscopic and macroscopic systems incorporate polarization based elements, the polarization plays a different role in each system. In the microscopic system, the polarization is used predominantly to eliminate specular reflection which otherwise would swamp the optical scatter signal we are attempting to measure. In the macroscopic systems, in contrast, polarization is predominantly used to be able to image deeper into the tissue.

To visualize molecular markers of breast cancer without inherent optical contrast, we have been assessing several types of absorbing, scattering, and emissive nanoparticles in Project 3. Because of continued regulatory concerns associated with quantum dots, even cadmium-free quantum dots, which we explored in Years 1 and 2 of the proposal, we are now almost completely focusing on gold-based nanomaterials. These materials are shaped or layered in different ways to provide optical properties matched to the systems developed in Project 1 and Project 2. The gold based materials used here, although at times layered, should not be confused with the nanoshells we have earlier optimized for photothermal therapy in a separate (now complete) DoD CDMRP effort (PI: Halas, Innovator Award) which was still active when this Era of Hope project was initiated. One of the most useful features of gold-based nanomaterials is the ability to exquisitely tune not only the resonance wavelength (color) of the material but also the absorption/scatter ratio, which determines whether the particle heats up when light is applied (for therapy) or scatters light (for imaging) or has some combination of both properties. Gold nanoparticles are designed to match the requirements of a particular application and wavelength of light and are thus not generally transferable across applications. We use the term "nanorod" to refer in general to all gold materials in which the optical response is controlled by the aspect ratio of the particle; we use the term "nanoshell" to refer to gold materials in which the optical response is controlled by the thickness of gold and dielectric layers. We have begun work on a material which in some ways can be thought of as an intermediary between these two in which we take a layered structure and insert into it an offset, non-symmetrical core. We have not yet physically realized these structures but recently published an initial paper describing the theory behind their optical properties. If we are successful in fabricating these structures, they may be useful material choices to consider as alternatives to nanorods for some imaging applications. Nanorods, while valuable as imaging agents when their two photon luminescence properties are exploited, have not been found to have sufficient scatter signal for use with the reflectance-based systems in Project 1, which require somewhat larger gold based nanomaterials with higher scattering cross-section. In this Era of Hope project, we are most interested in developing materials we can use in practical clinical settings with the instruments developed in Projects 1 and 2. For this purpose, we have found relatively large (>200 nm) gold nanoparticles are typically required.

Projects 1, 2, and 3 are linked through the intended use of these combinations of instruments and imaging agents for rapid, intraoperative tumor margin evaluation. Ultimately, it is envisioned that macroscopic imaging using a MOI device (Project 2) will be used to visualize the entire tumor while video rate microscopic imaging (Project 1) will be used to examine the margin region itself with contrast provided by the use of targeted imaging agents developed (Project 3). To provide an initial sense of what this might look like both macroscopic and microscopic images of tissue from a HER2+ patient are

included in the Project 3 results from the past year. HER2 is being used as the initial marker both because it allows ready identification of a cohort of patients which could ultimately be enrolled in pilot clinical studies and because expression is less variable than many other markers. However, it should be emphasized that there are no validated molecular markers for use in tumor margin applications, and the project should be regarded as a proof-of-principle study for this reason.

Project 1: Development of a Needle-Compatible Fiber Optic System for Breast Imaging

Reflectance Mode Imaging (Project 1: Task 1 and Task 2)

Prior year progress reports describe the motivation behind Project 1in detail. Briefly, we believe there is significant clinical motivation for considering the use of new types of optical imaging for breast cancer detection and treatment monitoring but that the limited penetration of light into breast tissue has impeded development of some of these applications. While many studies have been conducted using *ex vivo* breast tissue to demonstrate the promise of emerging optical techniques, there has been very limited work in *in vivo* translation of these methods largely because the limited light penetration makes these studies difficult. The largest project underway in our Era of Hope award has been aimed at overcoming this significant translational hurdle to the use of optical technologies in breast cancer applications. We believe that rather than be limited to applications where we bring the tissue to the light (by removing breast tissue from the body), it is important we bring the light to the tissue (by developing very small diameter microendoscopes inserted through needles of the size already used for fine needle aspiration or smaller). Additionally, we are focused on technologies that can provide direct high resolution images. While spectral i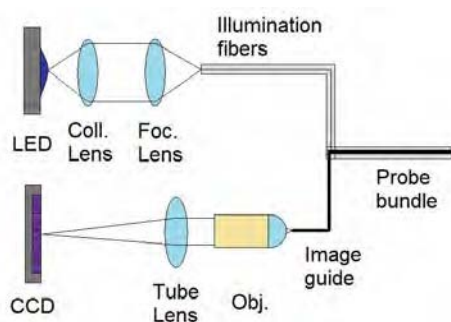nformation alone has already been shown to be of high diagnostic value, there is a need for modalities which can directly image tissue at high resolution as well. A large focus of our efforts over the past several years has been on refining our designs so the microendoscopes we develop can fit through the smallest needles possible while providing the best resolution and field of view. Although we describe these probes as "needle compatible," it should be emphasized that they do not need to be used through needle insertion in all applications. For instance, our tumor margin effort is based on surface imaging. It is just for applications where tissue must be accessed below the surface that we believe it is important there is a way to do this

Figure 1. The original optical design proposed. Note the separate use of illumination fibers for light delivery and an image guide for light collection. While this design worked, the outer diameter of the probe was not practical for clinical applications.

5

which is not possible with the several mm wide optical probes currently used in many applications.
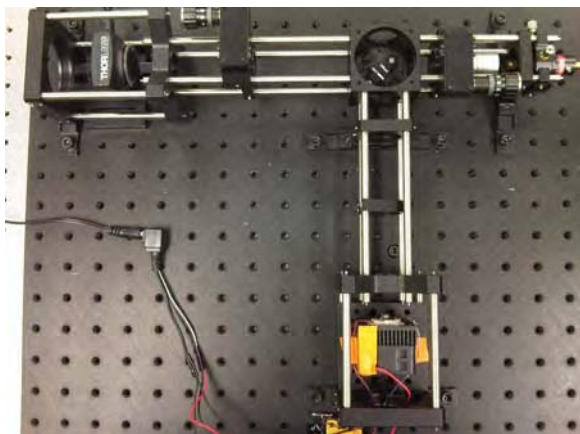

Figure 2. Photograph of the newest reflectance mode NCOB system using a polarizing beam splitter to combine the illumination and detection optical pathways at the image guide.

The latest improvement to the reflectance-mode needle-compatible optical biopsy (NCOB) system has benefited from lessons learned during the development of the multimodal optical imaging (MOI) system (Project 2) for macro-scale breast imaging. As opposed to the original design created in Year 1 (Figure 1) and the ring based design proposed in Year 2, our current design merges the illumination and detection optical pathways (Figure 2) using a simple and cheap polarizing beam splitter (PBS). The result is a probe that still has similar size to fine-needle aspiration biopsy needles. However, the signal strength and field of view (FOV) have been substantially increased. Just as importantly, these improvements have come with minimal increases in system cost and complexity. The current design of the system permits a reflectance mode imaging setup to be combined with fluorescence mode imaging setup (Project 1, Tasks 3 and 4), if desired, in a simple and straightforward manner. The two modes can then be used independently or in combination to take advantage of the potentially complementary information available in the images for breast cancer diagnosis and screening.

Improvements in Design over Prior Years
The key component of the NCOB system is the fiber image probe that must balance size, FOV size, signal strength, and signal-to-noise (S/N) ratio with additional considerations for cost and system complexity. One major previous obstacle was specular reflection from various optical-air interfaces in the system that overwhelmed the sample signal if one optical pathway was used for illumination and detection. However, separate illumination and detection optical pathways using separate coaxial optical fibers increased the size of the probe while reducing FOV and signal strength. Based on knowledge we acquired while building the MOI system (Project 2), the polarization of light has been used to solve the combined optical pathway problem. While in the MOI system the polarization of light is used to probe varying depths of tissue, in the NCOB system it is used to optically separate the illumination and detection optical pathways. This significantly reduces the design restrictions on the fiber probe itself. It is important to point out that a reflectance-based single fiber needle compatible microendoscope of

the type we have built in this project has never been developed before to the best of our knowledge.   A paper currently in press in Journal of Biomedical Optics (Sun et al, 2010) describes the design, and Rice University has filed a provisional patent on this idea.

The primary sources of specular reflection in the NCOB system are the air-glass interfaces of the lenses, the objective, and the image guide. Because light from specular reflection keeps its polarization, it can be separated from light scattered by the sample using a PBS or polarization filters. However, much of the light reflected by the sample also keeps its polarization and would be blocked from detector. By intentionally using a non-polarization maintaining image guide, we were able to alter the light reaching the sample so that it is no longer the same polarization as the specular reflection from sources before the image guide. This greatly increases the amount of signal that can be captured from the sample. On the other hand, there is still one more source of specular reflection from the fiber-air interface at the distal tip of the image guide probe, which is made worse by the polarization change in the image guide. This specular reflection is mitigated because the probe tip is in contact with tissue.   Tissue serves as an index matching substance to reduce the specular reflection. In this way, specular reflection from all sources up to the proximal tip of the image guide probe is significantly reduced while the light scattered by the sample is attenuated much less. Furthermore, this setup is simple and cheap, requiring only an additional PBS or two polarization filters and a beamsplitter (Figure 3) to allow a single illumination-detection optical pathway in the probe.
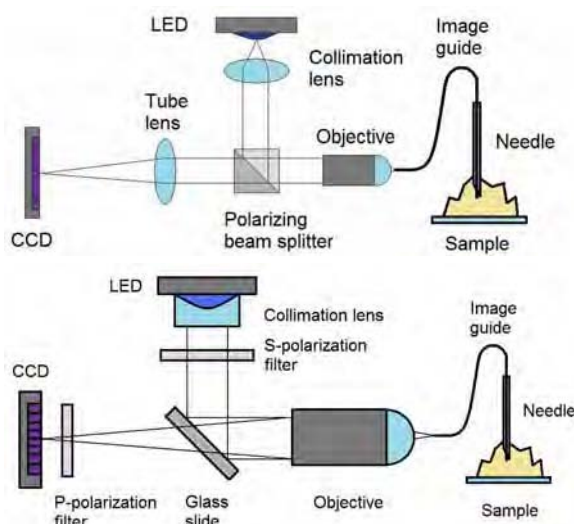
Figure 3. NCOB systems using a PBS (top) and two polarization filters and a glass slide (bottom). The PBS is more efficient at separating polarized light. The polarization filter setup is easy to customize.

Improvement in Performance

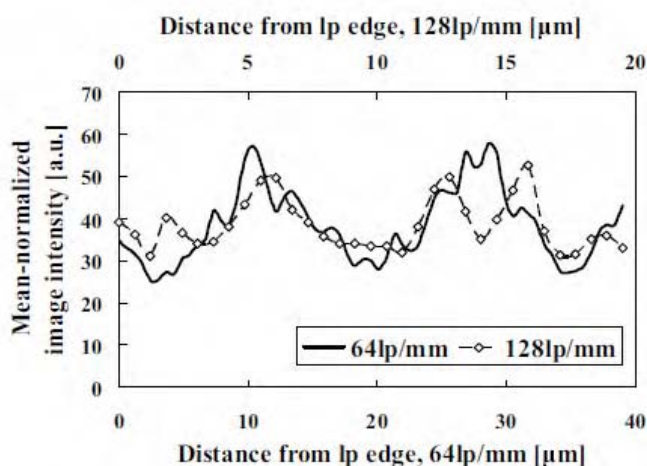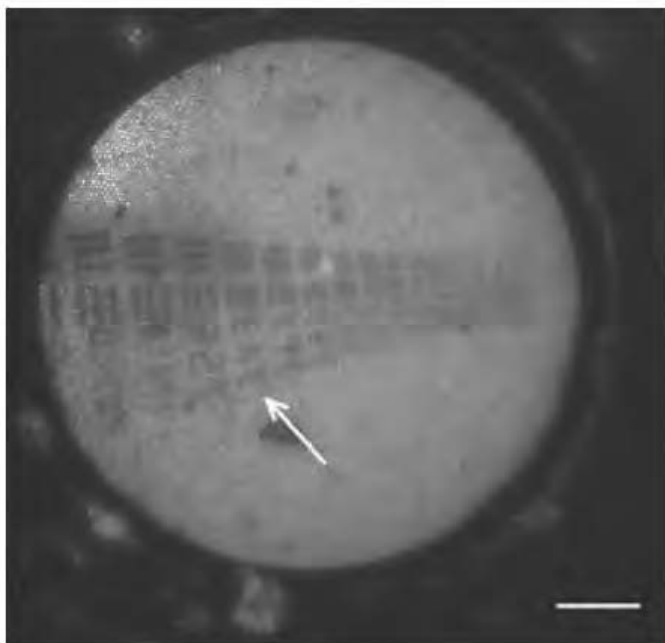Since the image guide probe was designed for simplicity and incorporates no additional optics, the probe must be in contact with the sample surface for the image to be in focus. When using separate illumination and detection fibers as we did in our prior version of this device, the signal from the sample relies on diffusely scattered light through the sample. The signal strength is so low in this case that it makes imaging inside bulk tissue difficult. Using earlier probe designs we were able to issue visualize large fat cells, the easiest breast imaging target, and to image suspensions of breast carcinoma cells but we could not image the tissue areas we were most interested in. Using the new polarization-based reflectance imaging system, the detection fibers are also the illumination fibers, and the areas of illumination are imaged directly. As can be seen from the figures in the Task 5 results section, we are beginning to be able to directly image intact tissue with no sectioning, no staining, or other preparation. This allows the system to be used under the conditions for which it was originally intended, ex vivo tissue imaging without sample preparation for tumor margin applications and in vivo tissue imaging without excision for diagnostic applications. In addition to the improvement in signal strength, use of the same image guide for both illumination and

Figure 4. Demonstration of resolution obtainable using the system developed in Year 3. Note the high (~3.5 micron) resolution obtainable demonstrated by the ability to resolve the line pairs indicated in the resolution chart shown above.

detection also reduces the required probe needle size for a given field of view. The needle size can be selected to suit situations where a larger field of view or a smaller needle is desired. We are currently using a 20-gauge needle probe with 333 um diameter field of view.   In the current design, we simply reduce field of view if we would like to use a smaller needle for a particular application.   Figure 4 demonstrates the resolution obtainable with the new system dramatically improved over previous performance.

Fluorescent-Based Needle Compatible Single Fiber Microendoscope (Project 1: Task 3 and Task 4)

To be able to consider both reflectance (scatter) and fluorescence based origins of image contrast, we have designed and constructed a complementary fluorescence based needle microscope endoscope.   The design of this system is shown in Figure 5.   The fiber microscope is assembled on a portable 18 × 24 × 1/2 inch^3 aluminum breadboard. An air-cooled royal blue batwing LED (Luxeon, model LXHL-NRR8) is selected as the illumination source. Illumination light emitted
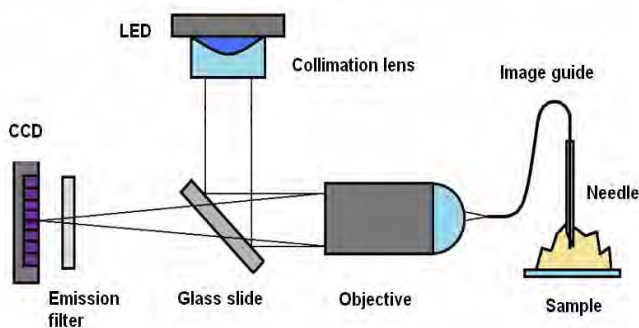

Figure 5. Schematic of the needle-compatible fluorescent fiber imaging system.

from the LED is collimated by an integrated collimation lens and reflected by a ~45°-positioned glass plate to project onto an infinitely corrected 10× objective lens (Newport, model: L-10x, 0.25NA). A multimode fiber coupler/positioner (Newport, model: F-915T) is utilized to mount the objective lens and a fiber chuck (Newport, model: FPH-DJ). With careful alignment, illumination light is focused into the incident end of a 450µm-outer-diameter fiber image guide (Sumitomo Electric, model: IGN-037/10) which is coupled by the fiber chuck. Finally, the imaging end of the image guide is inserted into the core of a 20-gauge needle and placed in contact with the samples. Light emitted by imaging samples is collected by the same illumination fiber and passed through the same objective lens and the glass plate as mentioned previously. A CCD color camera (Edmund Optics, model: EO-0813C) coupled with an emission filter (~540nm long-pass) is used for image acquisition. Clear fluorescent images collected from the imaging end can be obtained.

Potential Future Design Integrating Reflectance and Fluorescence Based Detection

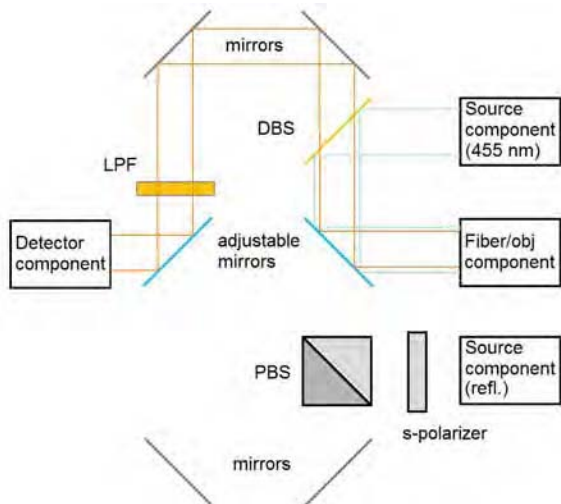Fluorescence and reflectance based imaging are complementary in many ways. Reflectance-based imaging (without the use of any added contrast agent) provides information on tissue architecture and cell morphology while fluorescence based imaging generally provides information on biochemistry. Molecular imaging agents may provide either type of optical signal. It is possible to integrate the two sets of designs described above into a single system. Figure 6 shows a diagram for a system of this sort. This is not a system we have built but is a system we would consider in the future if we obtain imaging results suggesting we want simultaneous fluorescence and reflectance images to enhance sensitivity and specificity. If only one type of image is needed, it is more straightforward to use the design shown in Figure 3 or Figure 5 for either reflectance or fluorescence, respectively. Here, we illustrate it is possible to integrate these into a single system if this proves desirable in the future..

Figure 6. Preliminary design of the combined reflectance and fluorescence mode NCOB system.

Evaluation of Needle Compatible Systems (Project 1: Task 5)
Reflectance Based System

We are in the process of evaluating system performance for imaging both cells and tissue. We first tested whether our system had sufficient resolving power and contrast to visualize individual cells (no dyes or other imaging agents of any kind used.) As shown in Figure 7, this is possible with the current design.
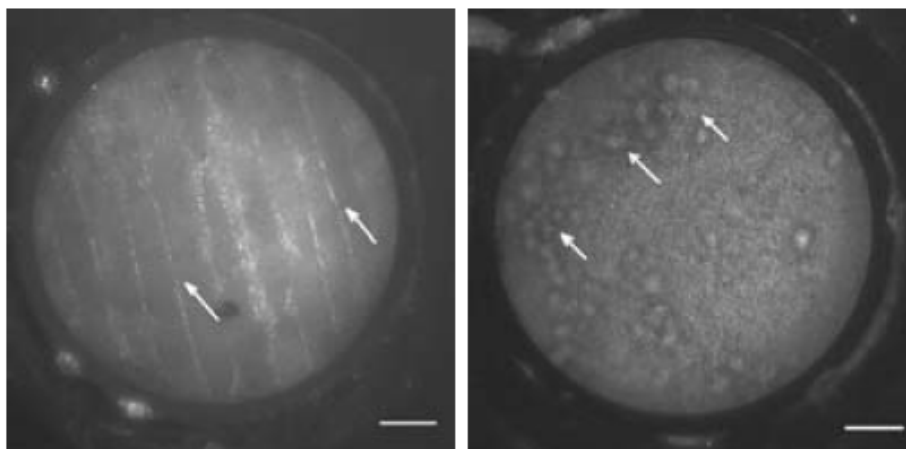

Figure 7. The microendoscope has sufficient resolving power to visualized individual cells. Left: onion cells imaged as an initial test. Right: Breast carcinoma cells.

Next, we evaluated the ability of the system to image intact excised human tissue (Figure 8). We have imaged both breast and oral tissue obtained from CHTN. Because of the high fat content of breast tissue, for initial testing it is easier to use oral tissue with higher cellular content. Unlike standard histology where tissue is being removed, fixed, sectioned, stained, and then imaged days later, we are showing direct imaging of intact tissue without sectioning or the use of any imaging agents. By performing only simple image processing (Figure 8, right), we are able to visualize both cell membranes (dark
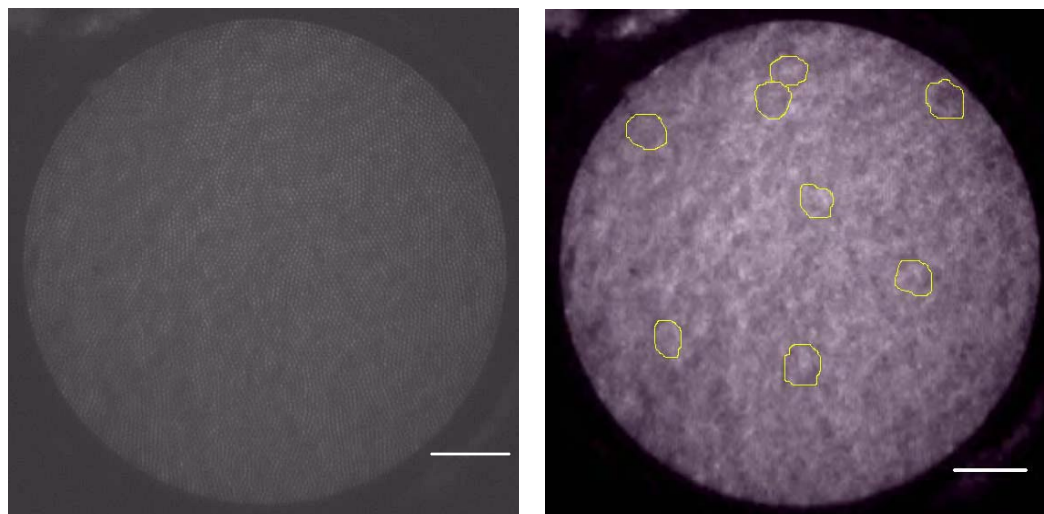

Figure 8. Human cancer tissue imaged by the NCOB system in filter setup (left). Simple image processing (right) allows the cell membranes and what we believe to be cell nuclei to stand out (right; cells marked with yellow outline). The cell membranes appear dark while the cell nuclei appear bright. The scale bars are 50 um.

circular shapes) and what we believe are cell nuclei (bright dots inside dark circular shapes). The use of this tissue reveals the ability to image the cell membrane and cell nuclei, the most important structural features we want to extract for cancer screening in tissue samples where much of the tissue morphology remains intact.

In addition to the more sophisticated nanoparticle based imaging agents being considered in Project 3, we have also been exploring the use of simple contrast agents already in routine
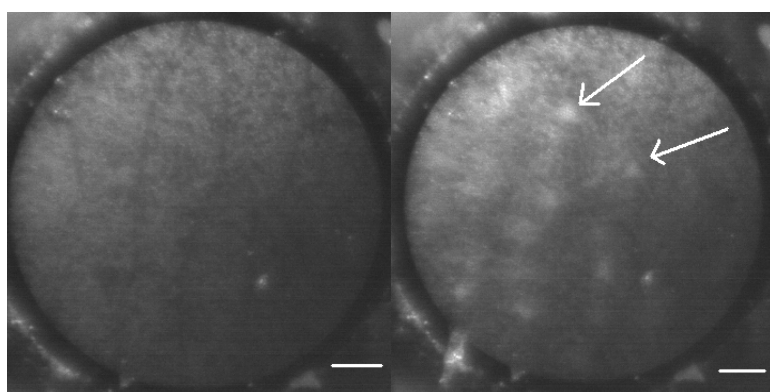

Figure 9. Cells before the application of acetic acid (left) and after application (right). Less than 1 min elapsed between the images. The scale bars are 50 um.

11

clinical use to enhance imaging capabilities. One of the first experiments we performed was the application of acetic acid to test what extent it would aid in making cell nuclei easier to visualize, one of our most significant challenges. Acetic acid (vinegar) is already widely used in colposcopy for cervical cancer to help establish suspicious areas by acetowhitening and is now used in dentists' offices as well with some commercial oral cancer screening devices. As can be seen in the images of cells in Figure 9, the application of acetic acid can dramatically improve nuclear visibility in cells in under a minute.

Fluorescence Based System

An initial test of the developed fluorescence-based fiber microscope was conducted using cultured SKBR3 human breast carcinoma cells incubated with 2-[N-(7-nitrobenz-2-oxa-1,3-diazol-4-yl)amino]-2-deoxy-d-glucose (2-NBDG). 2-NBDG is a fluorescent glucose analogue which accumulates preferentially in malignant cells. In this test study, the fiber bundle tip was immersed in PBS through a needle and focused onto a group of cells attached to the culture plate. As shown in Figure 10, cells incubated with 2-NBDG can be visualized with the florescent mode fiber microscope.
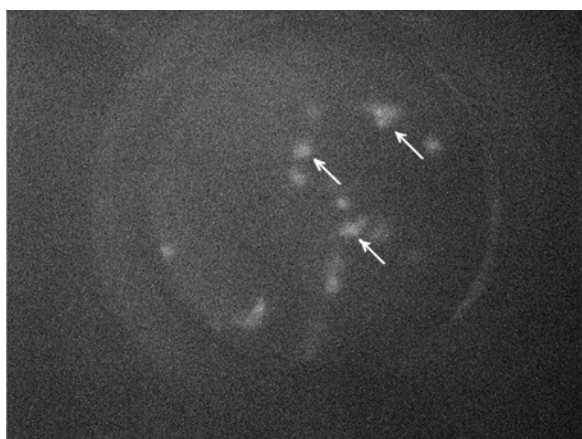
Figure 10. Endoscopic florescent image of cells incubated with 2-NBDG fluorescent dye obtained using the developed fluorescent fiber microscope, where the arrows indicate resolved single cells.

Ongoing and Future Work Underway in Project 1, Task 5

Currently two sets of experiments using the NCOB systems are being conducted in parallel. In one, imaging without any external contrast agents is being performed on breast cancer tissue samples. The goal of this study is two-fold. The first is the conclusive determination of cell membranes and cell nuclei in the images (and videos). This involves first being confident a human observer can identify these features and then developing automated processing algorithms for extraction. While we have successfully developing algorithms which allow extraction of cell boundaries (our Year 1 progress report provides details on the approaches being taken), it is more important than we be able to accurately estimate nuclear size. This has not yet been achieved. These will require more complex image processing and potentially additional optical improvements to the system. The other set of experiments involves testing of simple contrast agents already in clinical use to enhance the information content of the images in particular nuclear contrast. Our efforts in targeted molecular imaging are described in Project 3.

Project 2: Development of a Macroscopic Fluorescence/Reflectance Multi-Modal Optical Imaging (MOI) System (Task 1 and Task 2)

Figure 11. Multimodal optical imaging (MOI) system.

Multimodal optical imaging (MOI) technology can macroscopically screen large areas of tissue to identify cancerous regions and rapidly record this optical information without the need for biopsy. This technology has the potential to objectively identify and document disease related changes and aid in diagnosis or guide treatment including tumor resection. A multimodal optical imaging system has been designed and constructed for real-time clinical applications. Briefly, the MOI system is composed of a filtered xenon light source (Horiba Jobin Yvon Inc., Edison, NJ) and a filtered digital CCD camera (D300, Nikon) with a selected Nikon lens (AF Micro-Nikkor, 60mm, f/2.8D) (Figure 11). By selecting appropriate filter combinations, the MOI system provides various imaging modes, including white light imaging, polarized reflectance imaging, and fluorescence imaging. Both the light source and the camera are mounted on the same wheeled-stand to provide a fixed configuration of equipment with respect to the resected tissue sample. The wheeled stand allow easy maneuvering of the equipment in an operating room or other clinical environment. The MOI will be used to provide to guide placement of the microscopic fiber probes (Project 1) using the targeted imaging agents in Project 3.

Project 3: Development of Novel Targeted Imaging Beacons for Breast Imaging Applications (Task 3)

Tasks 1 and 2 of Project 3 were scheduled for and completed during Years 1 and 2 of the project. A paper published on Task 1 was included in last year's project report. The working version of a paper on Task 2 was included in last year's report, and the final published *Nanotechnology* paper is included in this year's report. During Year 3, we have focused on Task 3 which is the assessment of the most promising imaging agents. We have tentatively determined not to continue assessment of the cadmium free quantum dots because we received strong statements at both of the past two LINKS meetings from breast cancer patients attending the meetings that patients would be wary of clinical use of these agents even if regulatory issues were satisfactorily resolved. We had originally anticipated that by avoiding the use of cadmium, we would be able to address safety concerns, and our initial toxicity studies (included in Year 1 report) were promising. Based on the feedback received, we are focusing more strongly on gold

based materials already used clinically for other applications.

A variety of gold imaging agents are being evaluated in this project. All of these materials are quite different than the ~115-130 nm nanoshells with dual scattering/absorption properties whose initial development was funded by a separate DoD project which ended a few years ago (PI: Halas, Innovator Award). In last year's report, we included a new method for conjugation of antibodies to gold nanorods. We also included an image demonstrating imaging of targeted gold nanorods using two photon microscopy. Although these nanoparticles may be imaged in this way, doing so requires the use of a ~$100K laser and is not practical for the type of clinical applications we are interested in using the low cost instruments being developed in Project 1 and 2. However, scatter from nanorods can also be a source of contrast for imaging. The challenge in using nanorods in this way is whether sufficient signal exists for the particular scatter-based application. There is not a singular answer to this question as the answer depends on the specific imaging system being used, the dimensions of the nanorods, and the number of nanorods per targeted cell or tissue volume. Working in collaboration with two other groups at Rice University (the West lab and the Hafner lab), we have found that nanorods generally do not have sufficient contrast for the specific applications we are interested in pursuing through the Era of Hope project. To illustrate this, see the darkfield (scatter) images in Figure 12 of HER2+ breast carcinoma cells after incubation with either immunotargeted or non-specific nanorods. Note that there is no clear difference between control and experimental images when visualized using darkfield microscopy. Although one could reasonably ask whether the targeting itself might not have worked generating the negative results, the targeting is in fact clearly apparent when looking at the same sets of cells under two photon microscopy where nanorod signal is sufficient for imaging. The darkfield microscope used to obtain these images is able to collect much more scattered light than the small diameter microendoscopes developed in Project 1. If we cannot visualize the nanorods under darkfield illumination, we will not be able to see them using the Project 1 system. For this reason, we are now focusing on larger gold nanoparticles (AuNPs) designed to preferentially scatter light. We believe these nanoparticles will be the most appropriate choice for the tumor margin application described later in this section. It should be noted, however, that for applications based on systemic delivery, as opposed to the topical delivery being used in the tumor margin study, these AuNP would almost certainly be too large to be effectively delivered. Generating the scatter signal needed for these studies is determined largely by the overall size of the gold nanoparticle rather than layering or aspect ratio though all of these details come together to yield the final optical properties.
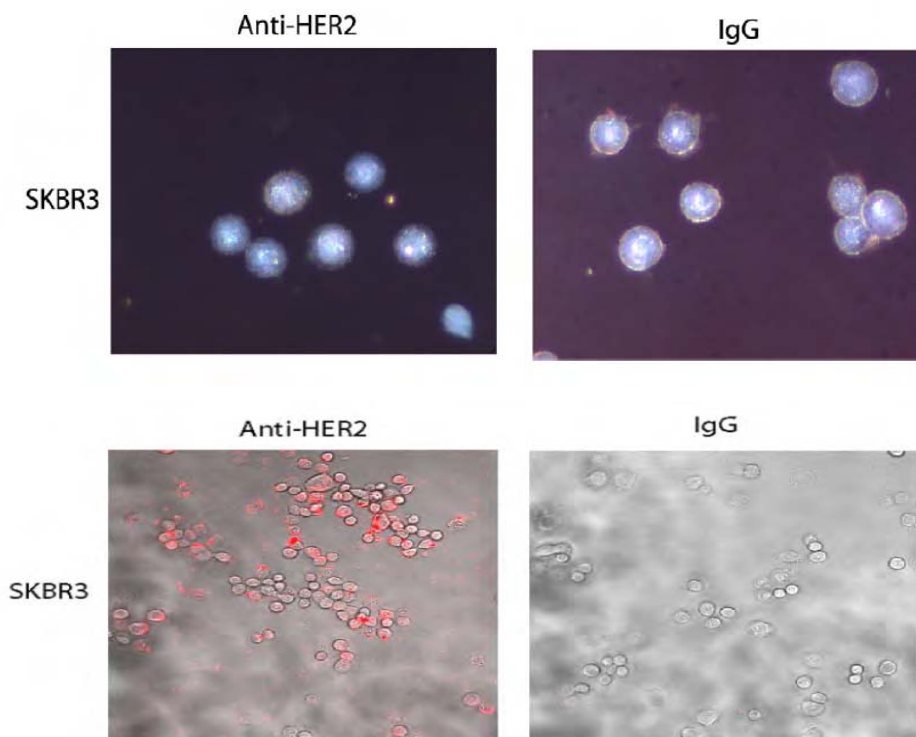
Figure 12. Top row: AntiHER2 (left) and non-specific (right) gold nanorods for imaging HER2+ cells using darkfield (scatter sensitive microscopy). Differences are not apparent comparing these images even though targeting is present. Targeting can be confirmed using a different form of imaging, two photon luminescence, as shown in the bottom row (data from last year). In this image, it is clear that gold nanorods are targeted to the cells as desired. However, they do not have strong enough optical signal to be visualized via darkfield.

Figure 13 is included to demonstrate that as the size of the AuNP is increased, the optical scatter signal rises, and it becomes much easier to use the materials as targeted contrast agents. Comparing the significant difference in the images in the middle and right column of Figure 13 to the hard to impossible to discern differences between the two pictures in the top row of Figure 12 demonstrate the importance of AuNP size.
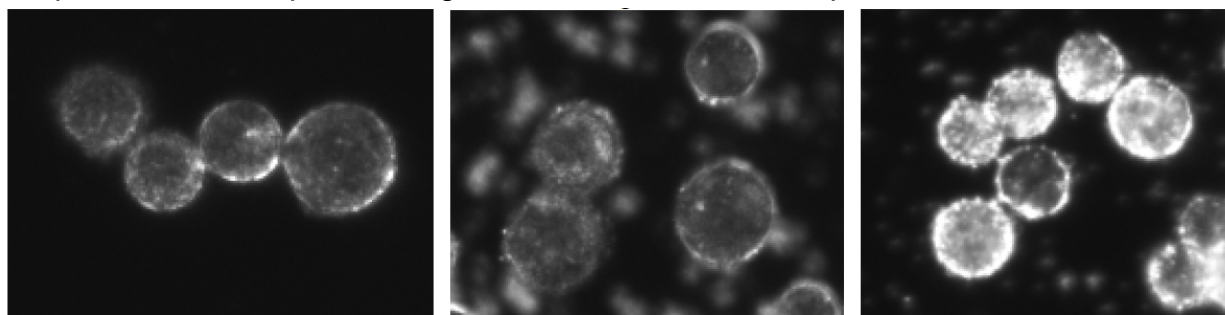

Figure 13. Left: SKBR3 cells alone. Middle: SKBR3 cells after incubation with AuNPs non-specifically targeted (IgG). Right: SKBR3 cells after incubations with antiHER2 AuNPs.

After determining what size AuNPs provide the necessary signal for imaging (>200 nm), we began assessing the use of immunotargeted AuNPs for tissue level molecular imaging applications initially by evaluating the enhanced optical signatures of *ex vivo* breast cancer tissue sections incubated with the nanoparticles. For these studies, we used normal breast tissue, HER2-negative cancerous tissue, and HER2-positive cancerous tissue specimens received flash frozen from the Cooperative Human Tissue Network (CHTN). Rice IRB approval was received for the use of this tissue and the DoD Claim of Exemption form was submitted. Specimens were thawed prior to being embedded in frozen section media. Sections were taken of all specimens at 20 microns and subsequently incubated with surface-modified AuNPs conjugated to anti-HER2 antibodies. Sequential sections were taken of all specimens at 5 microns (for standard histological processing). As shown in Figure 14, qualitative assessment of the imaging of normal (left column) and cancerous HER2- (middle column) tissue sections incubated with HER2-targeted AuNPs (Row B) showed little enhanced scattering. However the cancerous HER2+ tissue (right column) showed dramatically enhanced contrast after only 5 minutes of incubation with HER2-targeted AuNPs. Additional brightfield images (Row C) of the same tissue specimens validated the distribution of the AuNPs with respect to the tissue surfaces. The location and arrangement of the HER2-targeted NPs corresponded to the results obtained by performing immunohistochemistry (IHC) against HER2 (Row D). In order to demonstrate characteristic morphologic variations associated with normal and cancerous tissue, H&E stained sections (Row E) have also been included.
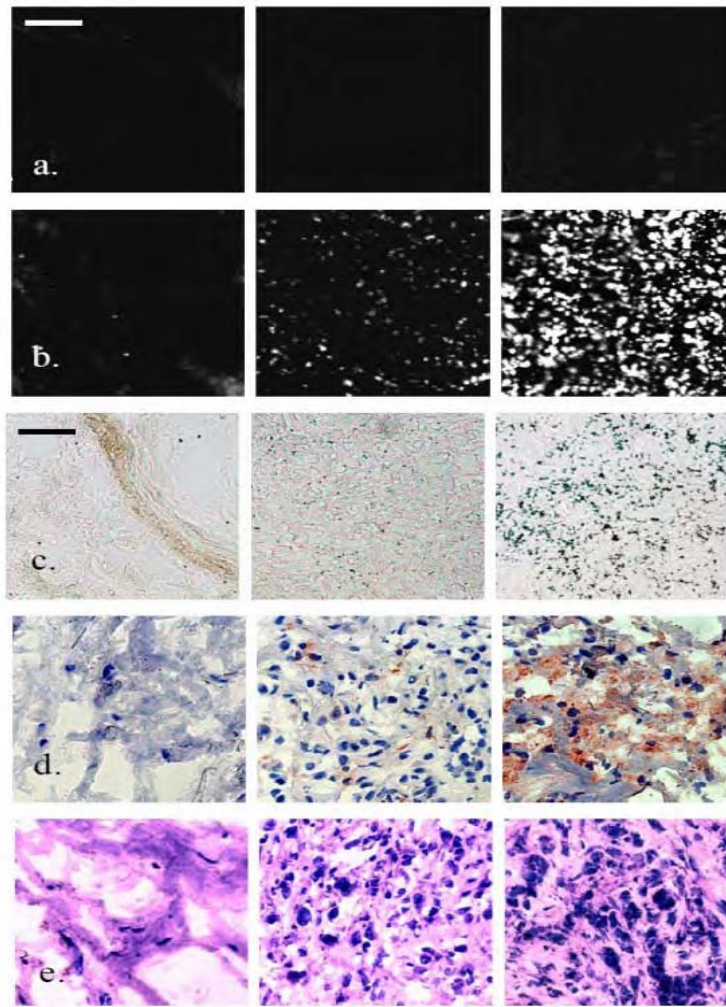
Figure 14. Reflectance (scatter based) images of normal (left), HER2-cancerous (middle), and HER2+ (right) cancerous human tissue samples alone (a) and after incubation with HER2-targeted AuNPs for 5 minutes (b). (c) Respective images from (b) taken under brightfield microscopy under 20x magnification. Respective (d) HER2/neu immunohistochemistry and (e) H&E results taken under brightfield under 20x magnification.. All scale bars represent 50 μm.

The results shown in Figure 14 essentially show that AuNPs can be used as an alternate label for HER2. In order to take the next step in translating this finding into a more immediate approach to obtaining diagnostic results in an operating room setting, studies are currently underway to examine the ability of targeted AuNPs to quickly (5 minutes) enhance contrast in resected breast tissue without physical sectioning. Both HER2+ cancerous tissue and HER2- cancerous tissue specimens were supplied by the CHTN and thawed prior to their use. A 5 mm (diameter) punch biopsy was used to extract samples of each tissue type in order to maintain size consistency. Sample thickness ranged from 1-2 mm. After incubation with either buffer or HER2-targeted AuNPs for 5 minutes at 37°C,
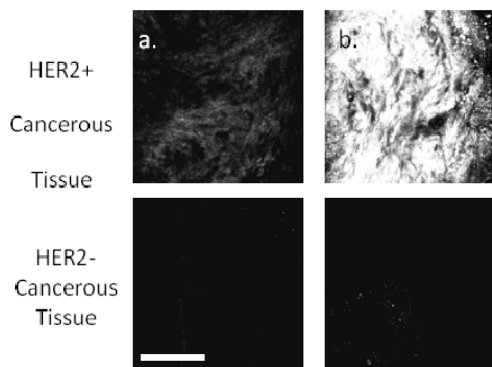

Figure 15. Preliminary results. Scatter-based images of HER2+ cancerous and HER2- cancerous human tissue samples incubated with (a.) buffer or (b.) HER2-targeted AuNPs for 5 minutes. Power at 0.4 mW. Scale bar = 0.13 mm.

samples were rinsed three times in 1xPBS and imaged without sectioning. As seen in Figure 15, scatter intensity is greatest when HER2-overexpressing tissue is incubated with HER2-targeted AuNPs (upper right image). In contrast, only low to no reflectance is evident in the buffer-only condition (upper left image) or for the negative control (lower row). These images provide preliminary evidence we will be able to use the reflectance based fiber bundle microscope (Project 1) in the manner we intend to scanning around the tumor margin looking for white spots indicative of areas of high HER2 suggesting more tissue may have needed to be removed.
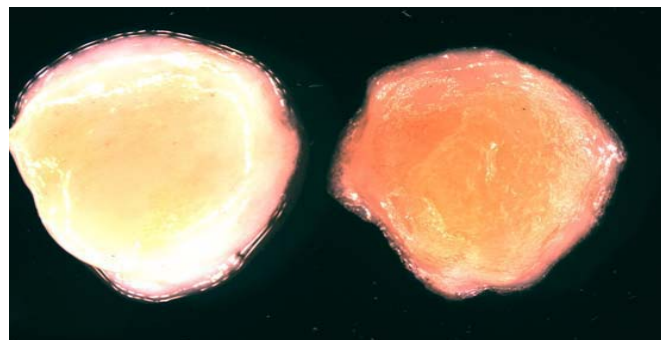
Figure 16. Macroscopic mages of HER2+ breast cancer tissue before (left) and after (right) five minute application of immunotargeted AuNPs. Magnification at 10x. This image on the right provides a sense of the type of macroscopic image we ultimately plan to obtain (although this entire sample is cancer) using the MOI imaging system being developed in Project 2 while the microscopic system being developed in Project 1 will be used to scan around the periphery of the tumor.

In addition to using scatter based imaging for microscopic visualization of AuNP targeting and HER2-overexpression, we are also exploring the use of scatter-based imaging for macroscopic evaluation of the same tissue. The macroscopic evaluation

would enable visualization of the entire tissue region at once and be used for guidance of the microscopic evaluation (generating a reddish glow from the AuNPs in cancerous areas in order to make it easier to visually differentiate the tumor from normal tissue).   If the number of suspicious regions that require further microscopic processing can be reduced, surgeons and pathologists can focus their attention and resources on areas that are most inconclusive.   To provide a sense of what these macroscopic images would look like, we evaluated HER2+ tissue from the CHTN and analyzed thawed, 5mm diameter samples from the same specimen.   Samples were incubated with either buffer or HER2-targeted AuNP at 37°C for 5 minutes.   Figure 16 demonstrates the enhanced contrast provided by the AuNPs after red wavelengths were enhanced through capabilities inherent in the camera's software.   This supports the potential ability to visualize AuNP targeting, and thus HER2-overexpression, through simple macroscopic imaging of whole tissue.   Although early in the evaluation process, these initial results support the use of AuNPs as promising contrast agents for potential rapid imaging applications at the point of care and will be a continued emphasis of our work moving forward.

Project 4:   Activatable Nanoparticles for Monitoring Radiation Therapy (closed)
This project was conducted during Years 1 and Year 2 only.   When the revised Statement of Work was submitted, the work scheduled for Years 3-5 of this effort was removed.   This change was made when it became clear that while the original idea behind this project was sound, the radiation levels required to create the optical signal changes needed were too high to be clinically relevant.   Essentially, we had proposed to directly monitor delivered radiation through optical signal changes created when the radiation interacted with gold nanoparticles causing a signal change when particular chemical bonds were broken.   We found the level of radiation required to create these changes were far higher than therapeutic levels used clinically.   Rather than continue this effort, we instead added the MOI imaging project (Project 2) needed to support the tumor margin effort and added tissue imaging studies throughout the project in addition to the cell based studies we had originally proposed (Projects 1 and 3).

Key Research Accomplishments

- The most significant accomplishment during the third year of this award was completion of the final design for a single fiber needle compatible reflectance microendoscope. This is a fiber optic microscope which can be threaded through even a very fine needle and can be used to directly image tissue with cellular resolution without having to stain the tissue in any way or remove it from the body.   The key to this small diameter device is a polarization based scheme to suppress specular reflectance.   By suppressing this unwanted optical signal, we were able to employ a single fiber bundle for both illumination and collection of light as opposed to our original microendoscope which required separate fibers for light delivery increasing the overall diameter because light delivery fibers were present in addition to the fiber bundle used for imaging.   The microscope, with an outer diameter of only a few hundred microns, has been demonstrated to have a lateral resolution of 3.5 microns.   This resolution allows individual cells to be visualized, and when sufficient contrast is present, some cell nuclei.

- The first paper describing the microendoscopes described above was recently submitted and accepted for publication in *Journal of Biomedical Optics*.   *Journal of Biomedical Optics* is widely regarded as the top publication venue for biomedical optics work.   Development of this probe was fully supported by the Era of Hope award.   The full pdf of the paper will be included in next year's progress report after it is published.

- A provisional patent application was filed with the USTPO by Rice University on May 3, 2010 to protect the technology above.   We plan to actively pursue commercialization of this device in order to bring the imaging benefits of this new approach to patients.   Although microendoscopes relying on exogenous fluorescent agents for imaging contrast have previously been demonstrated, this is the first reflectance-based single fiber microscope not requiring the use of any stain or imaging agent for contrast.

- After receiving approval from Rice and DoD for our tissue acquisition protocol and modification of our original Statement of Work, we are now obtaining normal and breast cancer tissue samples from the Cooperative Human Tissue Network enabling us to test our nanoparticle-based imaging agents in Project 3 under more clinically relevant conditions.   Despite the high number of papers published exploring diagnostic and therapeutic applications of nanotechnology in cancer, there is very little work evaluating the use of targeted nanoparticles in human tissue where a large number of factors come into play beyond those in cell based studies.

Reportable Outcomes

Journal Articles Acknowledging DoD Era of Hope Scholar Support
- Sun, J., Shu, C., Appiah, B., and <u>Drezek, R.</u> A Needle Compatible Single Fiber Reflectance Endoscope.   Accepted for publication in *Journal of Biomedical Optics.* In press (2010).

- Rostro-Kohanloo, B., Bickford, L., Payne, C., Day, E., Anderson, L., Zhong, M., Zhong, Lee, S., Mayer, K., Zal, T., Adam, L., Dinney, C., <u>Drezek, R.,</u> West, J., and Hafner, J. "Stabilization and Targeting of Surfactant-Synthesized Gold Nanorods." *Nanotechnology.* 20:434005 (2009).   (The submitted version of this paper was included last year but it had not yet been published.   The published version of the paper is included in this year's progress report.)

Provisional Patent Application Acknowledging DoD Era of Hope Scholar Support
- Reflectance fiber microscope for optical tissue biopsy (Rice University 2010-44). Inventors: Rebekah Drezek, Jiantang Sun, and Cheng Shu.   Filed May 3, 2010 with USTPO.   Patent application serial no 61/330,718.   Rebekah Drezek, Jiantang Sun, and Cheng Shu all have been directly supported by the DoD Era of Hope award.

Rice University Invention Disclosure Acknowledging DOD Era of Hope Scholar Support
- Reflectance fiber microscope for optical tissue biopsy (Rice University 2010-44). Inventors: Rebekah Drezek, Jiantang Sun, and Cheng Shu.

Book Chapter
- Bickford, L., Carpin, L, Sun, J., Hsu, K., <u>Yu, K.,</u> and <u>Drezek, R</u>.   Optical Technologies for Non-Invasive Functional and Molecular Imaging.   To be published as a chapter in the new edition of *Advanced Therapy of Breast Disease.*   In press (2010).   *This chapter does not report on our own research but rather provides a comprehensive overview of the use of the optical imaging technologies in breast cancer evaluation.   By serving as a commentator on optical imaging articles for Breast Diseases and authoring chapters for textbooks like this one, I hope to help the breast cancer community as a whole become more aware of both the potential and limitations of optical technologies.*

Abstracts
- Bickford, L., Yu, K., and <u>Drezek, R.</u>   Intraoperative Tumor Margin Detection Using Targeted Gold Nanoparticles, Baylor College of Medicine Translational Research Conference.   September 2009.

- Day, E., Bickford, L, <u>Drezek, R.,</u> and West, J.   Cancer Imaging and Thermal Therapy Facilitated by Nanoparticles and Multiphoton Microscopy.   ASME 2010 First Global Conference on Nanonengineering for Medicine and Biology.   Houston, TX.   Spring 2010.

- Langsner, R., <u>Drezek, R.,</u> and Yu, T.   A Fluorescent Deoxyglucose Analog for Detection of Cancer in Breast Tissue.   Rice Quantum Institute Summer Conference. August 2009.

Invited Presentations
- <u>Drezek, R.</u>   "Optically Activated Nanoparticles for Cancer Theranostics." Gordon Research Conference, Noble Metal Nanoparticles. Mount Holyoke College. Amherst, MA.   2010.

Jobs/Affiliation
- Rebekah Drezek became an Associate Member of the Baylor College of Medicine Duncan Cancer Center and is affiliated with the Lester and Sue Smith Breast Cancer Center

Awards
- Rebekah Drezek was awarded the 2009 Optical Society of America Adolph Lomb Medal for early career contributions to photonics

- Rebekah Drezek was named 2010 co-chair of Imaging for the Biomedical Engineering Society (BMES) Annual National Meeting

- Robert Langsner, a PhD student supported on this project has received a full travel award to present his work at the 2010 NSF Workshop on Advances in Breast Cancer

- Robert Langsner, a PhD student who has been supported on this project has received a NIH Biotechnology Training Fellowship for 2010 for his work developing optical techniques for identifying breast tumor margins

- Lissett Bickford, a PhD student working on this project has received the 2010 IBB Morse Graduate Fellowship for her work developing targeted gold nanoparticles for evaluating tumor margins

- Elizabeth Figueroa, a Rice undergraduate student who will be working on breast cancer molecular imaging, received a 2010 NSF IGERT Graduate Fellowship to attend Rice's PhD program in bioengineering

- Elizabeth Figueroa, an undergraduate student, receive a 2010 SPIE Optics Scholarship

- Joseph Chang, an undergraduate student working on this project, received the 2010 Bioengineering Undergraduate Research Excellence Award

CONCLUSIONS

Our research team is focusing the majority of its Era of Hope research efforts specifically in areas of breast cancer care where the combination of *miniaturized optical devices* and *molecular-specific imaging agents* offer the potential to address current gaps in care. There are two primary areas where I believe our technologies can make the biggest difference: *early detection* and *monitoring therapy.* Optical spectroscopy, implemented through small fiber optics, can provide clinically valuable information ranging from cellular metabolic status (via endogenous fluorescence) to nuclear size (correlated to optical scatter) to quantitative measurements of molecular markers (through targeted imaging agents under development in our lab). Most of our effort has focused on development of needle-compatible spectroscopic and direct imaging probes for breast cancer applications. The technology is being designed for clinical applications for which it is valuable to have a local high resolution imaging method to complement a more macroscopic imaging modality (for example, during ultrasound guided breast biopsy or optically guided tumor resection). Progressive design and evaluation of these needle-based technologies is **Project 1** of our DOD project. Important milestones over the past year include acceptance for publication in the top biomedical optics journal, *Journal of Biomedical Optics,* of our first paper in this area in addition to submission of a U.S. provisional patent application covering the technology developed. We have added in a new project, **Project 2**, to allow us to further develop a multi-modal macroscopic optical imaging device for use in guiding placement of the microscopic microendoscopes being developed in Project 1. To complement our imaging technology development projects, the second primary effort underway is development of molecular-specific optical imaging probes (**Projects 3**). Many similar probes developed to date have been suitable for lab-based but not clinical work. A challenge of most NP-based molecular contrast methods has been that conventional imaging protocols require incubation periods of over one hour. This is not clinically viable for either for our diagnostic or monitoring applications. We have developed protocols for imaging HER2 which provide sufficient contrast for imaging within five minutes. The fast imaging times we have been able to achieve open up the possibility of another type of breast cancer monitoring application: tumor margins assessment. Especially in community hospital settings, there is a critical need for new technologies for rapid intraoperative margins assessment. To be viable, a complete procedure must be accomplished in under 15-20 minutes. Much of the work already underway in **Project 3** is directly applicable to tumor margins assessment. Last year we modified our initial SOW to allow us to pursue the tissue-based studies needed to pursue this application. These studies have been initiated and will continue during the final two years of this project.

References

Sun, J., Shu, C., Appiah, B., and Drezek, R. A Needle Compatible Single Fiber Reflectance Endoscope. *Journal of Biomedical Optics.* In press (2010).

Rostro-Kohanloo, B., Bickford, L., Payne, C., Day, E., Anderson, L., Zhong, M., Zhong, Lee, S., Mayer, K., Zal, T., Adam, L., Dinney, C., Drezek, R., West, J., and Hafner, J. "Stabilization and Targeting of Surfactant-Synthesized Gold Nanorods." *Nanotechnology.* 20:434005 (2009).

The stabilization and targeting of surfactant-synthesized gold nanorods

The stabilization and targeting of surfactant-synthesized gold nanorods

Betty C Rostro-Kohanloo[1], Lissett R Bickford[2],
Courtney M Payne[4], Emily S Day[2], Lindsey J E Anderson[1],
Meng Zhong[3], Seunghyun Lee[4], Kathryn M Mayer[1], Tomasz Zal[5],
Liana Adam[3], Colin P N Dinney[3], Rebekah A Drezek[2],
Jennifer L West[2] and Jason H Hafner[1,4]

[1] Department of Physics and Astronomy, Rice University, 6100 Main Street, Houston,
TX 77005, USA
[2] Department of Bioengineering, Rice University, 6100 Main Street, Houston, TX 77005, USA
[3] Department of Urology, MD Anderson Cancer Center, 1515 Holcombe Boulevard, Houston,
TX 77030, USA
[4] Department of Chemistry, Rice University, 6100 Main Street, Houston, TX 77005, USA
[5] Department of Immunology, MD Anderson Cancer Center, 1515 Holcombe Boulevard,
Houston, TX 77030, USA

Abstract

The strong cetyltrimethylammonium bromide (CTAB) surfactant responsible for the synthesis
and stability of gold nanorod solutions complicates their biomedical applications. The critical
parameter to maintain nanorod stability is the ratio of CTAB to nanorod concentration. The
ratio is approximately 740 000 as determined by chloroform extraction of the CTAB from a
nanorod solution. A comparison of nanorod stabilization by thiol-terminal PEG and by anionic
polymers reveals that PEGylation results in higher yields and less aggregation upon removal of
CTAB. A heterobifunctional PEG yields nanorods with exposed carboxyl groups for covalent
conjugation to antibodies with the zero-length carbodiimide linker EDC. This conjugation
strategy leads to approximately two functional antibodies per nanorod according to fluorimetry
and ELISA assays. The nanorods specifically targeted cells *in vitro* and were visible with both
two-photon and confocal reflectance microscopies. This covalent strategy should be generally
applicable to other biomedical applications of gold nanorods as well as other gold nanoparticles
synthesized with CTAB.

Abbreviations

Ab	antibody
AF-Ab	Alexa Fluor labeled antibody
CCD	charge coupled device
CTAB	cetyltrimethylammonium bromide
EDC	1-ethyl-[3-dimethylaminopropyl]carbodiimide
ELISA	enzyme linked immunosorbent assay
HRP	horse radish peroxidase
LSPR	localized surface plasmon resonance
MES	2-(N-morpholino)ethanesulfonic acid (MES)
NHS	N-hydroxysuccinimide
PBS	phosphate buffered saline
PEG	poly(ethylene glycol)
PSS	poly(sodium 4-stryene-sulfonate)
WGA	wheat germ agglutinin

1. Introduction

Localized surface plasmon resonances (LSPR) of gold
nanoparticles result in strong optical absorption and scattering
at visible and near-infrared wavelengths [1]. These
optical properties are of considerable interest for biomedical
applications, since the plasmon resonance can affect localized
heating and light scattering, and since gold nanoparticles
are relatively inert in biological systems. Tunable gold
nanoparticles have been recently investigated for applications
in photothermal therapy, drug delivery and diagnostic
imaging [2–8]. Biomedical applications will ultimately rely
on the ability to target the gold nanoparticles specifically
to certain tissues or cell types with antibodies, aptamers
and peptides [9]. A variety of gold nanoparticle shapes
have been fabricated and investigated, including spheres [10],

shells [11], rods [12–18], cages [19, 20] and stars [21]. One nanoparticle synthesis that is particularly powerful and versatile is the growth of colloidal gold seeds in the presence of the surfactant cetyltrimethylammonium bromide (CTAB). This method produced gold nanorods at first in low yield [22], and then later in high yield [23, 24] with resonances in the near-infrared. Gold nanorods are of particular interest for biomedical applications due to their small size and potentially improved permeation into tissue, relative to larger tunable gold nanoparticles. However, gold nanorods and other shapes synthesized with CTAB are also stabilized by this strong surfactant, which is thought to form a bilayer on the nanoparticle surface [25]. If the CTAB is removed from solution, the nanorods immediately aggregate [17]. Several strategies have been developed to modify the surface chemistry of nanorods, including polyelectrolyte wrapping to bind the CTAB layer [26], displacement of the CTAB layer by a thiol-terminal polyethylene glycol (PEG) [17] and displacement by alkanethiols [27] and lipids [28]. Even with these options, manipulation and targeting of nanorods has proven difficult, although there has been some recent success with polyelectrolyte wrapping [9, 12, 29–37]. This report describes progress on three aspects of biological targeting of CTAB-synthesized gold nanorods. First, the sensitivity of nanorod stability to CTAB concentration has been carefully characterized. Second, a simple chemical strategy has been developed to create nanorod–antibody conjugates based on strong gold–thiol and amide bonds that specifically target cells. Third, optical imaging modalities to detect nanorods in cells have been compared.

2. Materials and methods

2.1. Nanorod synthesis

Gold nanorods were prepared as described previously [23, 24], but the procedure was scaled up to increase the quantity. All solutions were prepared fresh for each synthesis, except for the hydrogen tetrachloroaurate(III) (Sigma, #520918), which was prepared as a 28 mM stock solution from a dry ampule and stored in the dark. An aliquot of the stock solution was diluted to 10 mM immediately before use. Gold seed particles were prepared by adding 250 μl of 10 mM hydrogen tetrachloroaurate(III) to 7.5 ml of 100 mM cetyltrimethylammonium bromide (CTAB) (Sigma, #H9151) in a plastic tube with brief, gentle mixing by inversion. Next, 600 μl of 10 mM sodium borohydride (Acros, #18930) was prepared from DI water chilled to 2–8 °C in a refrigerator and added to the seed solution *immediately* after preparation, followed by mixing by inversion for 1–2 min. The pale brown seed solution was stable and usable for several hours.

　　The nanorod growth solution was prepared by adding the following reagents to a plastic tube in the following order and then gently mixing each by inversion: 425 ml of 100 mM CTAB, 18 ml of 10 mM hydrogen tetrachloroaurate(III) and 2.7 ml of 10 mM silver nitrate (Acros, #19768). Next, 2.9 ml of 100 mM ascorbic acid (Fisher, #A61) was added and mixed by inversion, which changed the solution from brownish-yellow to colorless. To initiate nanorod growth, 1.8 ml of seed
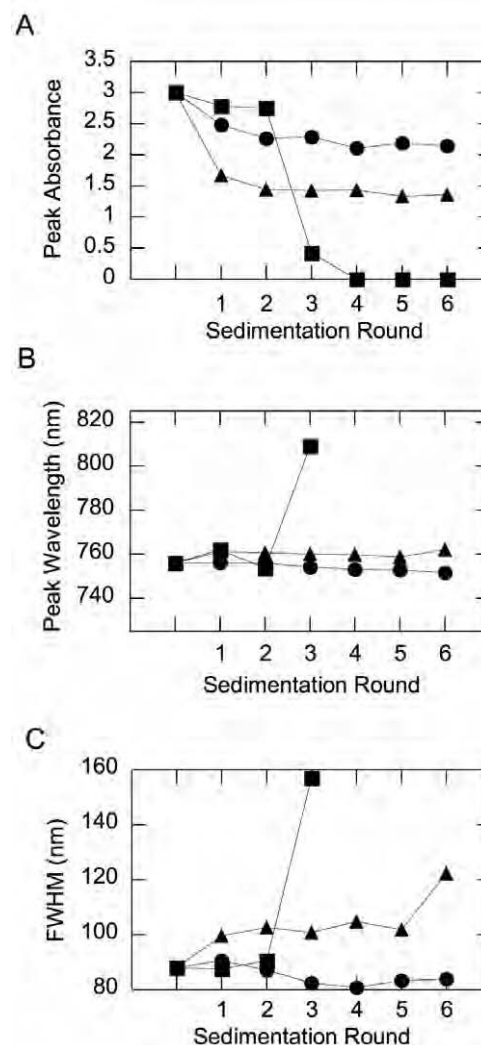

Figure 1. The evolution of the plasmon resonant peak of nanorod solutions after reduction of the CTAB concentration by sedimentation. The absorbance peak height (A), peak wavelength (B) and peak width (C) for CTAB-stabilized gold nanorods (■), anionic polymer-stabilized gold nanorods (▲) and PEGylated nanorods (●).

solution was added to the growth solution, mixed gently by inversion and left still for three hours. During this time, the color changed gradually to dark purple, with most of the color change occurring in the first hour.

2.2. Nanorod stabilization

Nanorod solutions were heated to 30 °C to melt CTAB crystals which form at room temperature, and therefore provide a known initial CTAB concentration of 100 mM. 5 ml aliquots were pelleted by centrifugation at 6000 rpm for 60 min. 4.5 ml of the clear supernatants were decanted and the pellets were resuspended with water. The nanorod solutions were pelleted again at 6000 rpm for 60 min and the clear supernatants were decanted. For anionic polymer stabilization, the nanorod pellets were resuspended with 4.5 ml of a solution containing 30 mg ml^{-1} poly(sodium 4-styrene-sulfonate) (PSS, Aldrich, #243051) and 1 mM NaCl. For PEGylation, the nanorod pellets were resuspended with 4.5 ml
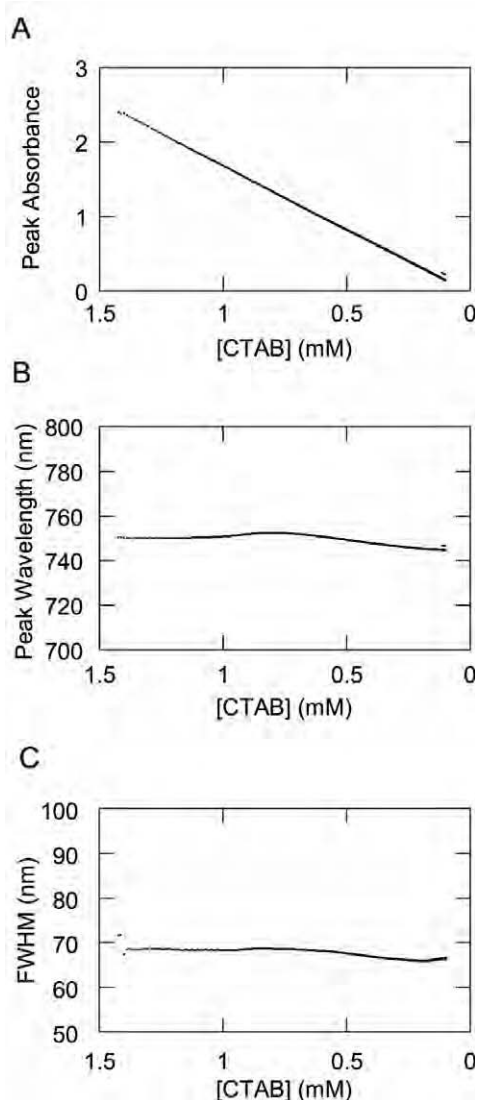
Figure 2. The evolution of the plasmon resonant peak height (A), wavelength (B) and width (C) of a nanorod solution during dilution with water.

of a solution containing 200 μM K_2CO_3 and 10 μM mPEG-SH (Nektar Therapeutics, #2M4E0H01). For both stabilization methods, the nanorod solution was incubated overnight at room temperature. Subsequent rounds of sedimentation, decantation and resuspension with water were then carried out as described above to lower the CTAB concentration.

2.3. CTAB dilution

CTAB dilution was carried out by two methods. For the data in figure 1, the CTAB was diluted by subsequent rounds of sedimentation, decantation and resuspension with water as described in the preceding section, except that no stabilizing agent was applied. For the data in figure 2, a 600 μl aliquot of nanorods diluted to 1.4 mM CTAB was put in a custom 9 ml cuvette for spectral analysis. The plasmon resonant spectral extinction was monitored as water was added to the solution at 20 μl min^{-1} with a pipette pump.

2.4. Chloroform extraction

A separation funnel was filled with 100 ml of chloroform and 10 ml of nanorod solution which contained 30 mM CTAB. The mixture was vigorously shaken and allowed to separate overnight. The aqueous nanorod solution was extracted and 500 μl aliquots were placed in test tubes. To these tubes were added increasing quantities of chloroform for a second extraction: 0, 50, 100, 150, 200, 250 and 300 μl. After vigorous mixing, these were allowed to separate overnight. The aqueous nanorod solutions were then removed and analyzed.

2.5. Nanorod bioconjugation

Nanorods were stabilized with the heterobifunctional linker α-thio-ω-carboxy poly(ethylene glycol) (Iris Biotech, #HOOC-PEG-SH) by the PEGylation method described above and resuspended in 100 mM 2-(N-morpholino)ethanesulfonic acid (MES) buffer (Sigma, #M-0164) at pH 6.1. The nanorods were concentrated by sedimentation to a volume of 100 μl with an absorbance value greater than 10 at the LSPR peak wavelength. 96 mg of 1-ethyl-[3-dimethylaminopropyl]carbodiimide (EDC, Sigma, #1769) and 29 mg of N-hydroxysuccinimide (NHS, Sigma, #1306762) were added to 10 ml of MES buffer, mixed and then 10 μl of this solution was immediately added to the 100 μl nanorod solution. This mixture was allowed to sit for 15 min, during which 0.5 ml of 2-mercaptoethanol was diluted into 14.5 ml MES buffer. After 15 min incubation, 10 μl of the diluted 2-mercaptoethanol was added to the nanorod solution. This mixture was allowed to sit for 10 min, after which 400 μl of the antibody solution at 2 mg ml^{-1} in PBS pH 7.1 was added. This final 500 μl NR/Ab solution was incubated for 2 h at room temperature. Finally, the NR–Ab conjugates were separated from excess reactants and by-products by sedimentation at 10 000 rpm, decantation and resuspension of the pellet in PBS buffer.

2.6. Fluorimetry

The procedure above was followed with an Alexa Fluor 488-labeled rabbit IgG (AF-Ab, Invitrogen, #A11059). Upon completion, the AF-Ab–NR conjugates were put through subsequent rounds of sedimentation, 90% decantation and resuspension in PBS. The supernatants and the final AF-Ab–NR conjugate solutions were analyzed in a Horiba Jobin-Yvon FluoroLog-3 fluorimeter with CW xenon excitation. The free AF-Ab in the supernatants served as a standard curve to determine the concentration of AF-Ab bound to the nanorods.

2.7. Nanoparticle ELISA

Gold nanorods conjugated to mouse anti-human HER2 antibodies (NeoMarkers, #MS-301-PABX) were incubated with HRP-labeled anti-mouse IgG (Sigma, #A4416) for 1 h. Nonspecific reaction sites were blocked with a 3% solution of bovine serum albumin (BSA). Nanorods were rinsed twice by sedimentation and resuspension in 3% BSA to remove any unbound IgG. The HRP bound to the nanorod conjugates was

developed with 3, 3′, 5, 5′-tetramethylbenzidine dihydrochloride (Sigma, #T3405) and compared with an HRP anti-mouse IgG standard curve by determining the absorbance at 450 nm with a spectrophotometer.

2.8. Nanorod targeting

Anti-HER2 nanorod conjugates were incubated with two cell types: the HER2-overexpressing epithelial breast cancer cell line SK-BR-3 and the normal mammary epithelial cell line MCF10A (American Type Culture Collection). The SK-BR-3 cells were grown in McCoy's 5A medium supplemented with 10% fetal bovine serum (FBS) and 1% penicillin–streptomycin and maintained at 37 °C in a 5% CO_2 atmosphere. The MCF10A cells were cultured in mammary epithelial basal medium (MEBM) supplemented with a BulletKit (Clonetics) and also maintained at 37 °C in 5% CO_2. Both cell lines were prepared for the experiment by putting 6×10^5 cells in chambered cover slips and allowing them 30 min to attach to the surface. The cells were rinsed once with PBS, then incubated with nanorod conjugates for 1 h in 5% CO_2 at 37 °C. The LSPR peak absorbance of the nanorod conjugate solutions was 1.5. After the incubation, cells were rinsed $3\times$ with $1\times$ PBS and then the appropriate cell medium was added prior to imaging. The cells were imaged by two-photon microscopy at $50\times$ with 780 nm illumination and 400–700 nm detection.

KU7 cells were grown in MEM medium supplemented with 10% fetal bovine serum (FBS) and 1% penicillin–streptomycin and maintained at 37 °C in a 5% CO_2 atmosphere. The cell line was prepared for the experiment by putting 4×10^5 cells on cover slips and allowing them 24 h to attach to the surface. Prior to the treatment, the cell media was changed to OptiMEM (Roche Biochemicals) and nanorod-C225 conjugates were added for 4 h. After 4 h, the OptiMEM medium was changed to MEM medium supplemented with 10% serum and incubated in 5% CO_2 at 37 °C atmosphere for another 20 h. Twenty minutes prior to fixation, the cells were rinsed once with warm PBS, then incubated with 100 nM Alexa-488-wheat germ agglutinin (WGA) and left for 10 min in the cell incubator for WGA cellular internalization. After 10 min the cells were rinsed three times with warm PBS, fixed in 1:1 methanol:ethanol at 20 °C for 10 min, then washed three times with cold PBS and mounted on slides using slow-fade antifade. All reagents were purchased from Molecular Probes. Imaging was carried out with a Leica SP5RS AOBS confocal microscope using a $63\times/1.4$ objective. Nanorods were detected with 633 nm illumination in reflection mode. WGA-AF488 was excited at 488 nm and detected at 495–530 nm.

3. Results

3.1. Nanorod stability

In order to determine the critical CTAB concentration required for nanorod stability, nanorod solutions were heated to melt the CTAB crystals and provide a well-defined initial concentration of 100 mM. Aliquots of nanorods were then pelleted by sedimentation, 90% of the clear supernatant was removed and
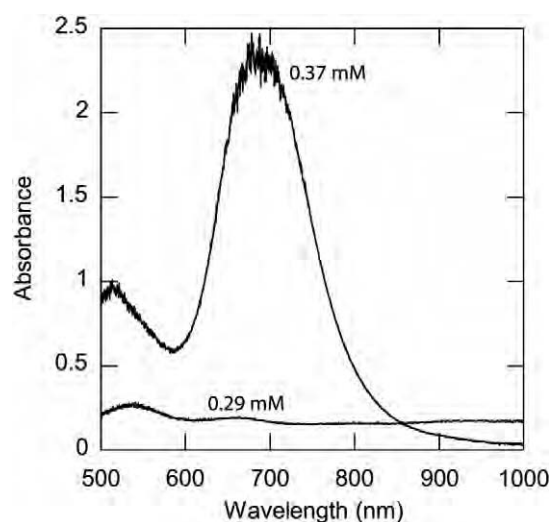

Figure 3. The plasmon resonant extinction spectra of nanorod solutions at two CTAB concentrations achieved by chloroform extraction. The nanorod concentration was 0.5 nM.

the nanorod pellets were resuspended to their initial volume with water. In this way the CTAB concentration was reduced by a factor of 10 on each round of sedimentation. Note that the quantity of CTAB bound to the nanorod surfaces is a negligible fraction of this initial CTAB concentration[6]. The LSPR peak wavelength, width and height were recorded after each round of sedimentation and are plotted in figure 1. There was essentially no nanorod aggregation, i.e. no LSPR peak height reduction, broadening, or redshift, until the third round of sedimentation. Therefore, nanorod aggregation is expected to occur somewhere between 1 and 0.1 mM CTAB.

To further characterize the critical CTAB concentration, the LSPR spectrum of a nanorod solution was monitored during slow dilution with water (figure 2). As expected, the LSPR peak absorbance decreased as the nanorod concentration was reduced. However, the LSPR peak wavelength and width were not affected, indicating that there was no aggregation, although the CTAB concentration was reduced to below 50 μM. This apparent inconsistency with the results of figure 1 reveals that it is the ratio of CTAB concentration to nanorod concentration that determines stability, not the CTAB concentration alone, which is typical for surfactant-stabilized colloids. To further confirm this point, CTAB was removed from a nanorod solution without reducing the nanorod concentration by extraction with chloroform. As seen in figure 3, there was a critical CTAB concentration at which aggregation occurred. Based on our own measurement of the distribution ratio for CTAB between water and chloroform, the aggregation occurred between 370 and 290 μM CTAB. Given that the nanorod concentration was 0.5 nM, the critical CTAB/nanorod concentration ratio was approximately 740 000. Note that this number of CTAB molecules per

---

[6] Consider the typical conditions of a nanorod solution with $l = 50$ nm, $d = 15$ nm nanorods at an LSPR peak absorbance of 1, which corresponds to a nanorod concentration of 0.2 nM. The nanorod surface area would be 3063 nm^2. The CTAB bilayer packing area is 22 Å^2. Therefore, each nanorod would contain 14 000 CTAB molecules on its surface, taking up only 2.8 mM of the CTAB concentration.

Table 1. Zeta potential measurements to confirm surface chemistry modification.

Nanoparticle	ZP (mV)
NR–CTAB	+83
NR–S-PEG-COOH	−19
NR–S-PEG-Ab	−6

nanorod is much larger than the amount of CTAB needed to simply coat the nanorods with a surfactant bilayer (see the footnote above), so the dynamic interactions between CTAB in solution and in the bilayer must be important for nanorod stability.

Nanorods were stabilized by displacement of the CTAB with a thiol-terminal polyethylene glycol (mPEG-SH), and by wrapping the CTAB bilayer with polystyrene sulfonate (PSS). The LSPR peak wavelength, width and height after successive rounds of sedimentation are displayed in figure 1 to probe the effectiveness of these stabilizers. While the unstabilized nanorods aggregated after the third round of sedimentation as described above, both PEGylation and polyelectrolyte stabilization were effective. However, PEGylation maintained a narrower LSPR peak, indicating a reduced degree of aggregation relative to polyelectrolyte stabilization.

3.2. Nanorod bioconjugation

To form stable nanorod bioconjugates, a heterobifunctional polyethylene glycol with thiol and carboxyl end groups (HOOC-PEG-SH) was applied. Nanorod stabilization with HOOC-PEG-SH yielded identical results to mPEG-SH in figure 1. The carboxy-terminal nanorods were conjugated to antibodies using the zero-length crosslinker EDC stabilized by NHS [38]. Standard procedures for EDC protein crosslinking were followed [39], with the following modifications for the unique properties of the carboxy-terminal nanorods. First, since the functionalized nanorod surfaces contain no amines, there is no chance of nanorod aggregation due to amide bond formation between nanorods, which minimizes the criticality of the initial EDC exposure. Second, to avoid the need for buffer exchange or sedimentation, the change in pH from 6.1 for activation to 7.1 for conjugation was accomplished by diluting the nanorods into a larger volume of antibody solution. Finally, sedimentation was performed (rather than buffer exchange) to remove excess reactants and products from the nanorod solution.

As a means to confirm the altered nanorod surface chemistry at various stages, zeta potential measurements (Malvern Zetasizer Nano) were performed on gold nanorods in the original CTAB, after stabilization with HOOC-PEG-SH, and finally after Ab conjugation. The results, presented in table 1, are consistent with the cationic, anionic and zwitterionic surface charges, respectively, associated with these three states of nanorods.

To characterize the final product, nanorods were conjugated to AF-Ab for fluorimetric analysis. After the steps described above, the nanorod conjugates were put through successive rounds of sedimentation, 90% decantation and
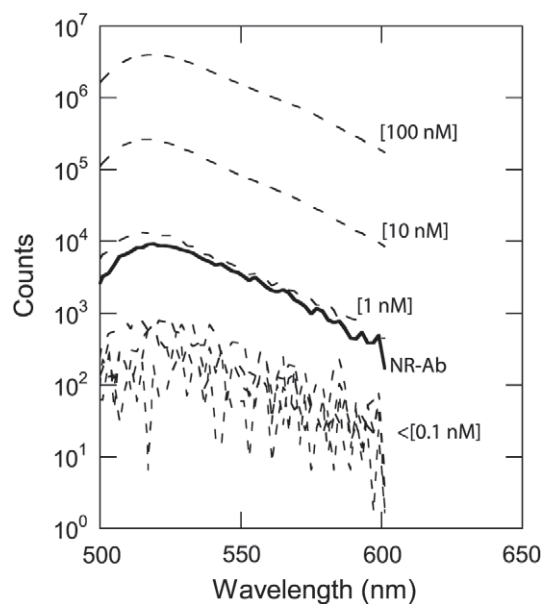

Figure 4. Fluorimetric analysis of gold nanorod conjugates. The dashed curves display the signal from free labeled antibodies in solution at the stated concentrations. The solid curve displays the signal from nanorod conjugates.

resuspension in buffer to dilute the unbound AF-Ab by factors of ten. Fluorimetry of unbound AF-Ab in the decants, shown in figure 4, serves as a standard curve and reaches the background fluorescence noise floor by the fourth round at an AF-Ab concentration of 0.1 nM. Fluorimetry of the nanorod conjugates solution indicated a nanorod-bound AF-Ab concentration of 1 nM, which yields approximately two antibodies per nanorod given a nanorod concentration of 0.5 nM based on the LSPR extinction peak [17].

To further characterize the nanorod conjugates, a nanoparticle ELISA was performed [40]. This method is similar to a traditional ELISA except that the immunosorbent surface is that of the nanoparticles in solution. The nanoparticle ELISA yielded 2.28 ± 0.05 antibodies per nanorod, in reasonable agreement with the fluorimetry results. A simultaneous ELISA on nanorods prepared with mPEG-SH, and therefore no capture antibodies, yielded 0.68 ± 0.2 antibodies per nanorod. This signal may be an artifact due to chemisorption of the label antibody to the available gold surface on the nanorods.

3.3. Nanorod targeting and imaging

Nanorod conjugate targeting was tested with two *in vitro* systems. First, nanorods were conjugated to anti-HER2 and also to rabbit IgG as a control. Each conjugate was incubated with both the HER2-overexpressing epithelial breast cancer cell line SK-BR-3 and the normal mammary epithelial cell line MCF10A for 30 min simultaneously and under identical conditions. The cells were washed and immediately imaged live by two-photon luminescence, which highlights the presence of gold particles [18], as well as phase contrast to show the cell locations. Figure 5 demonstrates that only the specific antibody/cell combination produced a significant level
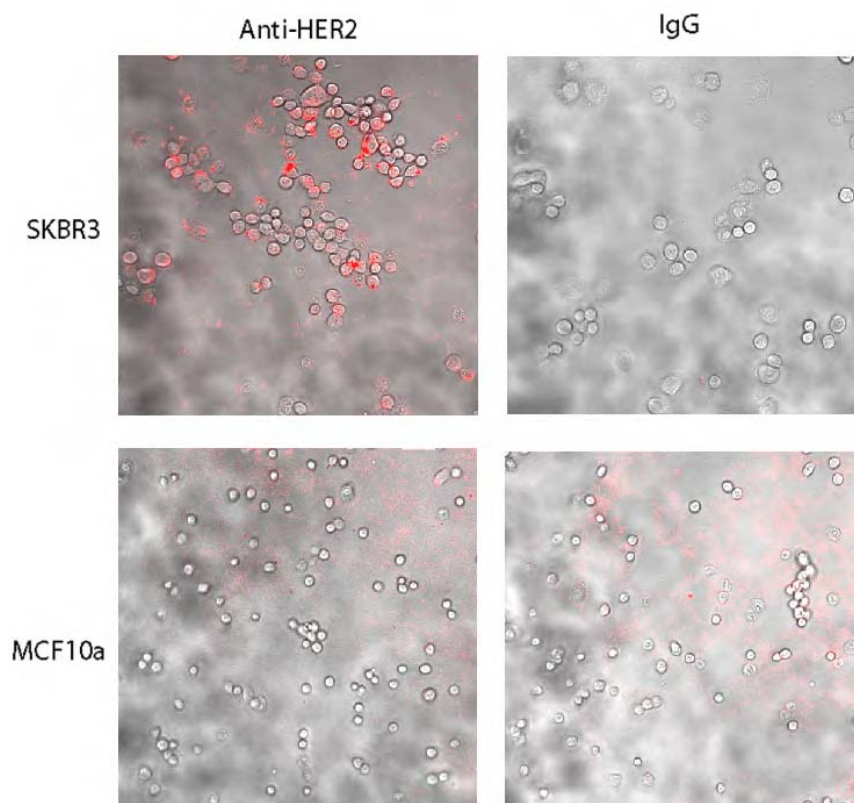
Figure 5. Nanorod conjugate targeting. Phase contrast shows the cell locations in grayscale, and two-photon luminescence is displayed in red. Binding was only observed for the anti-HER2 conjugates and SKBR3 cells.
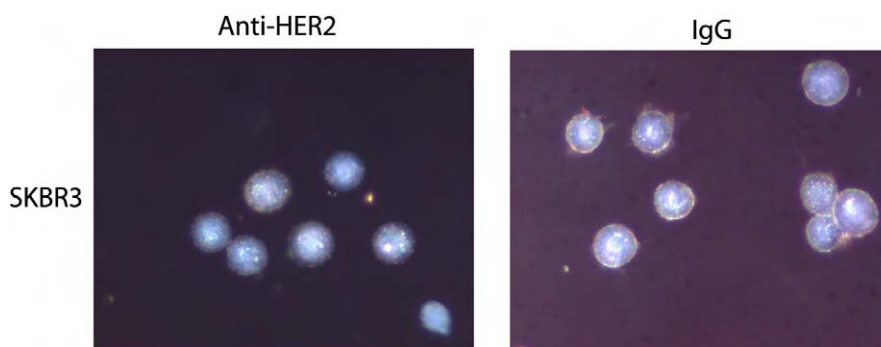

Figure 6. Dark-field microscopy images of the same samples as in figure 5.

of nanorod binding to the cells. Figure 6 displays dark-field images of targeted and control cells from the same sample. The nanorods were not visible. To gauge their visibility in dark-field microscopy, isolated nanorods were deposited on glass substrates near alignment marks and easily visible spherical gold nanoparticles so that optical microscopy and AFM could be performed on the same area (see figure 7). The nanorod was not detectable on either a high-sensitivity monochromator or color CCD cameras.

The conjugation method was also tested with C225 and human IgG as a control. In this case, the nanorod conjugates were incubated with the KU7 bladder cancer cell line. The nanorods were imaged by confocal reflectance and the cells were visualized with a fluorescent WGA label. The C225

conjugates were more strongly associated with KU7 cells than the control IgG conjugates, as seen in figure 8.

4. Discussion

It is well known that the CTAB surfactant responsible for gold nanorod synthesis is also required to maintain colloidal stability. However, the CTAB concentration at which colloidal stability is lost has not been well characterized. This is due to several factors. First, to reduce the CTAB concentration in a nanorod solution, it is often removed by sedimentation of the nanorods into a pellet, decantation of the CTAB solution and resuspension of the nanorod pellet in water. If this procedure is not performed analytically, the CTAB concentration is
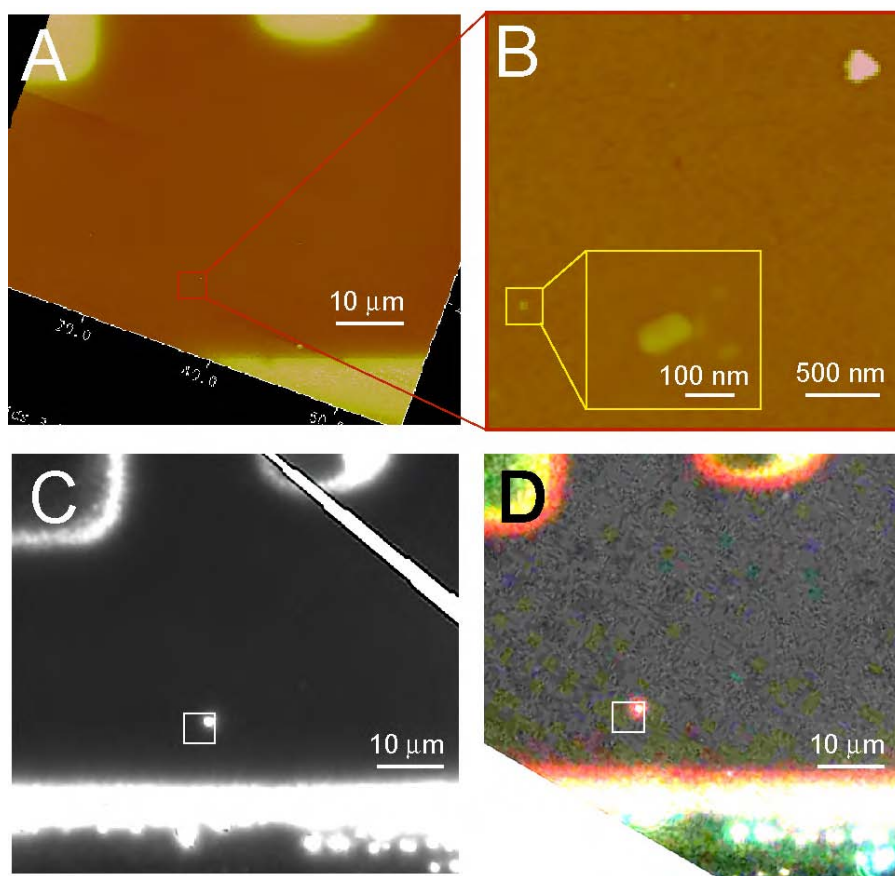
Figure 7. Dark-field microscopy images of a single gold nanorod on glass. The first AFM image (A) shows a region near alignment marks that are also visible in the optical images ((C) and (D)). A zoomed AFM image (B) reveals a large nanosphere in the upper right (triangular shape is a tip artifact) and a nanorod in the lower left. The nanorod is clearly revealed in the inset. Its size is exaggerated by the tip. The true size is approximately 50 nm length and 15 nm width. Dark-field images captured with a high-sensitivity CCD (C) and color CCD (D) clearly show the nanosphere, but show no sign of the nanorod in the expected region, even with significant contrast enhancement. The inset boxes in (A), (C) and (D) are all shown at the same size and position.
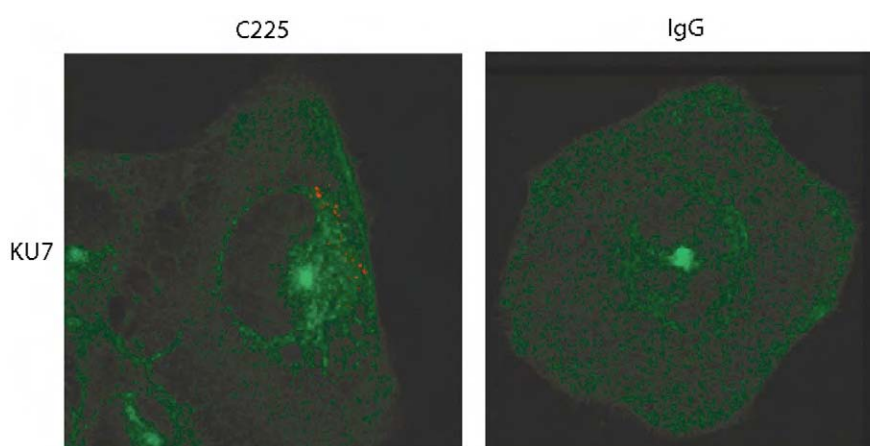

Figure 8. *In vitro* nanorod imaging by confocal reflectance. WGA-AF488 fluorescence shows the cell location in green and confocal reflectance at 633 nm is shown in red. Nanorod binding is only observed for the specific C225 conjugates and KU7 cells.

reduced by an unknown amount. Second, nanorod synthesis is carried out at 100 mM CTAB, which is above the saturation concentration at room temperature. Upon storage, some of the CTAB crystallizes, leaving an unknown concentration in the nanorod solution drawn from the solution phase. Finally, attempts at spectroscopic or other analyses of the CTAB concentration are hindered by micellization and association with gold and silver ions in solution.

That the nanorods were found to be entirely stable to a CTAB concentration below 1 mM may confound the development of methods to stabilize nanorods, since the CTAB may stabilize the nanorods when it is thought to have been

removed. Nanorod stabilization outside of the CTAB solution is further complicated by several factors. First, the aggregation occurs quite suddenly when the CTAB concentration falls below the critical value, as seen in figure 3. Second, the fact that it is the ratio of CTAB to nanorod concentration that determines stability, rather than the CTAB concentration alone, means that the critical CTAB concentration for a given sample will depend on the nanorod concentration. Third, since CTAB forms a bilayer on the nanorod surface, it is likely that the available nanorod surface area is critical for stability rather than the nanorod concentration. Therefore, the critical CTAB concentration for a given sample also depends on nanorod size. This significant variability of the critical CTAB concentration between samples may in part account for reproducibility issues in stabilizing gold nanorods and forming bioconjugates.

We previously described a strategy to stabilize gold nanorods with a thiol-terminal polyethylene glycol (mPEG-SH) which displaces the CTAB bilayer so that CTAB can be reduced to an arbitrarily low concentration and the nanorods remain in solution [17]. Nanorods can also be stabilized by wrapping them with anionic polymers which are attracted to the cationic CTAB bilayer, as well as by forming multiple polyelectrolyte layers [26]. Figure 1 displays a comparison of the effectiveness of these methods for stabilizing nanorods. Interestingly, after the first and second rounds of sedimentation, the sample with no stabilizing treatment maintained the best spectrum, although aggregation occurred rapidly thereafter. The data demonstrate that, upon removal of CTAB, PEGylation via the thiol–gold bond results in higher yields and a narrower LSPR linewidth than electrostatic stabilization. This spectroscopic result is in agreement with previously reported microscopic characterizations of nanorod substrates. PEGylated nanorod solutions yield highly monodisperse nanorods when deposited on glass substrates [17], while electrostatic wrapping leads to aggregated nanorods [26].

Most gold nanorod targeting experiments to date have been carried out by stabilizing the CTAB-capped gold nanorods with polyelectrolytes, then non-covalently binding antibodies or other targeting agents to the nanoparticles by simply mixing them together [12, 29, 31–33, 35, 36]. This is similar to the original strategies developed to bind antibodies to citrate-capped gold nanoparticles for immunoelectron microscopy [41]. The binding is likely due to weak electrostatic and hydrophobic interactions between the nanoparticles and antibodies. To create more stable nanorod bioconjugates, the strategy described here relies on an amide bond between the linker and antibody, and a strong gold–thiol bond [42] between the linker and nanorod. In some cases polyelectrolytes with exposed carboxyl groups for amide bond formation with antibodies have been employed [30, 37]. In one case an alkanethiol was used in a similar manner to the bifunctional PEG described here [43]. While alkanethiols are more readily available, their low solubility in aqueous solutions required hours of sonication at elevated temperature to achieve sufficient concentration to displace the CTAB bilayer. Although more complicated, conjugates based on gold–thiol and covalent bonds will likely be more stable for

in vivo applications. Furthermore, we have found the methods described here to be quite reproducible despite the strength of the original gold–CTAB interaction [12]. Tests of the nanorod zeta potential follow the intended surface chemistry, with a negative potential for carboxy-terminated nanorods and a near-neutral potential for the zwitterionic protein conjugates. The fluorimetric assay yields approximately two antibodies per nanorod and the ELISA assay demonstrates that a large fraction of these antibodies are active. Finally, figures 5 and 8 demonstrate successful targeting in two cell types with different antibodies.

We have also investigated the effectiveness of different imaging modalities to visualize nanorods in and around cells. As described previously [18], the images based on two-photon luminescence in figure 5 clearly reveal nanorods in the specific sample. Dark-field microscopy is a much simpler modality that can yield striking images of plasmon resonant nanoparticles [44]. However, the optical scattering which provides dark-field contrast is a strong function of nanoparticle size. Furthermore, the size range at which nanoparticles become visible by dark-field is tens of nanometers, similar to the range of nanoparticles that have been pursued for biomedical applications. Issues of visibility are also sensitive to the illumination and imaging numerical apertures, spectral range, nanoparticle aggregation and background scattering from cells. Therefore, one must be cautious when interpreting nanoparticle targeting results by dark-field microscopy. For example, the dark-field images from figure 6 reveal no evidence of scattering by the nanorods, even though the two-photon images from figure 5 confirm the presence of nanorods. In this case the single 50 nm × 15 nm nanorods do not scatter sufficiently to be visible against the scattering from cells. To further confirm this point, dark-field images of a single nanorod on a glass substrate are displayed in figure 7. Although the location of a single gold nanorod relative to alignment marks is confirmed by atomic force microscopy, one finds that the nanorod is not visible in the dark-field images taken with either a color CCD camera or a back-illuminated electron multiplying CCD camera. If single nanorods are not visible on a flat glass substrate, it is not surprising that they are not visible in the higher background images of cells in figure 6. There are many methods to increase the nanorod imaging signal and contrast without resorting to two-photon luminescence, such as spectrally filtering the scattered light, exciting with monochromatic illumination at the plasmon resonant wavelength and using a higher numerical aperture condensers and objectives. Figure 8 reveals that confocal reflectance microscopy, with monochromatic illumination at the LSPR wavelength and reduced background signal, is sufficient to detect nanorods in cells.

5. Conclusions

To maintain colloidal stability, it is the ratio of CTAB to nanorod concentration that must be maintained. Here, the critical CTAB:nanorod ratio was found to be approximately 740 000:1. The CTAB layer can be displaced by thiol-terminal PEG, or wrapped by polyelectrolytes. However,

gold–thiol PEGylation results in higher yields and more monodisperse nanorod samples when the CTAB is removed. A bifunctional PEG with thiol and carboxyl end groups results in carboxy-terminal PEGylated nanorods which can be conjugated to antibodies via a carbodiimide linking agent. Fluorimetry and ELISA assays reveal approximately two antibodies per nanorod. The nanorod conjugates demonstrated specific targeting in two different antibody/cell systems. Two-photon luminescence and confocal reflectance microscopies successfully imaged the nanorods in cells.

Acknowledgments

References

[1] Link S and El-Sayed M A 1999 Spectral properties and relaxation dynamics of surface plasmon electronic oscillations in gold and silver nanodots and nanorods *J. Phys. Chem.* B **103** 8410–26

[2] Liao H, Nehl C L and Hafner J H 2006 Biomedical applications of plasmon resonant metal nanoparticles *Nanomedicine* **1** 201–8

[3] Jain P K, Huang X H, El-Sayed I H and El-Sayed M A 2008 Noble metals on the nanoscale: optical and photothermal properties and some applications in imaging, sensing, biology, and medicine *Acc. Chem. Res.* **41** 1578–86

[4] Murphy C J, Gole A M, Stone J W, Sisco P N, Alkilany A M, Goldsmith E C and Baxter S C 2008 Gold nanoparticles in biology: beyond toxicity to cellular imaging *Acc. Chem. Res.* **41** 1721–30

[5] Lal S, Clare S E and Halas N J 2008 Nanoshell-enabled photothermal cancer therapy: impending clinical impact *Acc. Chem. Res.* **41** 1842–51

[6] Bikram M and West J L 2008 Thermo-responsive systems for controlled drug delivery *Expert Opin. Drug Deliv.* **5** 1077–91

[7] Tong L, Wei Q S, Wei A and Cheng J X 2009 Gold nanorods as contrast agents for biological imaging: optical properties, surface conjugation and photothermal effects *Photochem. Photobiol.* **85** 21–32

[8] Hleb E Y, Hu Y, Drezek R A, Hafner J H and Lapotko D O 2008 Photothermal bubbles as optical scattering probes for imaging living cells *Nanomedicine* **3** 797–812

[9] Pirollo K F and Chang E H 2008 Does a targeting ligand influence nanoparticle tumor localization or uptake? *Trends Biotechnol.* **26** 552–8

[10] Sokolov K, Follen M, Aaron J, Pavlova I, Malpica A, Lotan R and Richards-Kortum R 2003 Real-time vital optical imaging of precancer using anti-epidermal growth factor receptor antibodies conjugated to gold nanoparticles *Cancer Res.* **63** 1999–2004

[11] Loo C, Lowery A, Halas N, West J and Drezek R 2005 Immunotargeted nanoshells for integrated cancer imaging and therapy *Nano Lett.* **5** 709–11

[12] Javier D J, Nitin N, Roblyer D M and Richards-Kortum R 2008 Metal-based nanorods as molecule-specific contrast agents for reflectance imaging in 3D tissues *J. Nanophoton.* **2** 023506

[13] Yu C X, Nakshatri H and Irudayaraj J 2007 Identity profiling of cell surface markers by multiplex gold nanorod probes *Nano Lett.* **7** 2300–6

[14] Eghtedari M, Oraevsky A, Copland J A, Kotov N A, Conjusteau A and Motamedi M 2007 High sensitivity of *in vivo* detection of gold nanorods using a laser optoacoustic imaging system *Nano Lett.* **7** 1914–8

[15] Huff T B, Hansen M N, Zhao Y, Cheng J X and Wei A 2007 Controlling the cellular uptake of gold nanorods *Langmuir* **23** 1596–9

[16] Chen C C, Lin Y P, Wang C W, Tzeng H C, Wu C H, Chen Y C, Chen C P, Chen L C and Wu Y C 2006 DNA-gold nanorod conjugates for remote control of localized gene expression by near infrared irradiation *J. Am. Chem. Soc.* **128** 3709–15

[17] Liao H and Hafner J 2005 Gold nanorod bioconjugates *Chem. Mater.* **17** 4636–41

[18] Wang H, Huff T B, Zweifel D A, He W, Low P S, Wei A and Cheng J-X 2005 *In vitro* and *in vivo* two-photon luminescence imaging of single gold nanorods *Proc. Natl. Acad. Sci. USA* **102** 15752–6

[19] Cang H, Sun T, Li Z Y, Chen J Y, Wiley B J, Xia Y N and Li X D 2005 Gold nanocages as contrast agents for spectroscopic optical coherence tomography *Opt. Lett.* **30** 3048–50

[20] Skrabalak S E, Chen J, Au L, Lu X, Li X and Xia Y 2007 Gold nanocages for biomedical applications *Adv. Mater.* **19** 3177–84

[21] Nehl C L, Liao H W and Hafner J H 2006 Optical properties of star-shaped gold nanoparticles *Nano Lett.* **6** 683–8

[22] Jana N R, Gearheart L and Murphy C J 2001 Wet chemical synthesis of high aspect ratio cylindrical gold nanorods *J. Phys. Chem.* B **105** 4065–7

[23] Sau T K and Murphy C J 2004 Seeded high yield synthesis of short Au nanorods in aqueous solution *Langmuir* **20** 6414–20

[24] Nikoobakht B and El-Sayed M A 2003 Preparation and growth mechanism of gold nanorods (NRs) using seed-mediated growth method *Chem. Mater.* **15** 1957–62

[25] Nikoobakht B and El-Sayed M A 2001 Evidence for bilayer assembly of cationic surfactants on the surface of gold nanorods *Langmuir* **17** 6368–74

[26] Gole A and Murphy C J 2005 Polyelectrolyte-coated gold nanorods: synthesis, characterization and immobilization *Chem. Mater.* **17** 1325–30

[27] Sun Z H, Ni W H, Yang Z, Kou X S, Li L and Wang J F 2008 pH-controlled reversible assembly and disassembly of gold nanorods *Small* **4** 1287–92

[28] Niidome Y, Honda K, Higashimoto K, Kawazumi H, Yamada S, Nakashima N, Sasaki Y, Ishida Y and Kikuchi J 2007 Surface modification of gold nanorods with synthetic cationic lipids *Chem. Commun.* 3777–9

[29] Tong L, Zhao Y, Huff T B, Hansen M N, Wei A and Cheng J X 2007 Gold nanorods mediate tumor cell death by compromising membrane integrity *Adv. Mater.* **19** 3136

[30] Popovtzer R, Agrawal A, Kotov N A, Popovtzer A, Balter J, Carey T E and Kopelman R 2008 Targeted gold nanoparticles enable molecular CT imaging of cancer *Nano Lett.* **8** 4593–6

[31] Huang X H, El-Sayed I H, Qian W and El-Sayed M A 2007 Cancer cells assemble and align gold nanorods conjugated to antibodies to produce highly enhanced, sharp, and polarized surface Raman spectra: a potential cancer diagnostic marker *Nano Lett.* **7** 1591–7

[32] Huang X H, El-Sayed I H, Qian W and El-Sayed M A 2006 Cancer cell imaging and photothermal therapy in the near-infrared region by using gold nanorods *J. Am. Chem. Soc.* **128** 2115–20

[33] Hu R, Yong K T, Roy I, Ding H, He S and Prasad P N 2009 Metallic nanostructures as localized plasmon resonance enhanced scattering probes for multiplex dark-field targeted imaging of cancer cells *J. Phys. Chem.* C **113** 2676–84

[34] Hauck T S, Ghazani A A and Chan W C W 2008 Assessing the effect of surface chemistry on gold nanorod uptake, toxicity, and gene expression in mammalian cells *Small* **4** 153–9

[35] Durr N J, Larson T, Smith D K, Korgel B A, Sokolov K and Ben-Yakar A 2007 Two-photon luminescence imaging of cancer cells using molecularly targeted gold nanorods *Nano Lett.* **7** 941–5

[36] Ding H, Yong K T, Roy I, Pudavar H E, Law W C, Bergey E J and Prasad P N 2007 Gold nanorods coated with multilayer polyelectrolyte as contrast agents for multimodal imaging *J. Phys. Chem.* C **111** 12552–7

[37] Agarwal A, Huang S W, O'Donnell M, Day K C, Day M, Kotov N and Ashkenazi S 2007 Targeted gold nanorod contrast agent for prostate cancer detection by photoacoustic imaging *J. Appl. Phys.* **102** 064701

[38] Grabarek Z and Gergely J 1990 Zero-length crosslinking procedure with the use of active esters *Anal. Biochem.* **185** 131–5

[39] Hermanson G T 1996 *Bioconjugate Techniques* 1st edn (New York: Academic) p 785

[40] Lowery A R, Gobin A M, Day E S, Halas N J and West J L 2006 Immunonanoshells for targeted photothermal ablation of tumor cells *Int. J. Nanomed.* **1** 149–54

[41] Geoghegan W D and Ackerman G A 1977 Adsorption of horseradish-peroxidase, ovomucoid and antiimmunoglobulin to colloidal gold for indirect detection of concanavalin-a, wheat-germ agglutinin and goat antihuman immunoglobulin-g on cell-surfaces at electron-microscopic level—new method, theory and application *J. Histochem. Cytochem.* **25** 1187–200

[42] Nuzzo R G, Zegarski B R and Dubois L H 1987 Fundamental-studies of the chemisorption of organosulfur compounds on Au(111)—implications for molecular self-assembly on gold surfaces *J. Am. Chem. Soc.* **109** 733–40

[43] Eghtedari M, Liopo A V, Copland J A, Oraevslty A A and Motamedi M 2009 Engineering of hetero-functional gold nanorods for the *in vivo* molecular targeting of breast cancer cells *Nano Lett.* **9** 287–91

[44] Mock J J, Barbic M, Smith D R, Schultz D A and Schultz S 2002 Shape effects in plasmon resonance of individual colloidal silver nanoparticles *J. Chem. Phys.* **116** 6755–9

A Needle-Compatible Single Fiber Bundle Image Guide Reflectance Endoscope

Running title: Needle compatible reflectance fiber endoscope

Jiantang Sun[1], Chenghao Shu[1], Benjamin Appiah[2], Rebekah Drezek[1, 2,*]

[1]Departments of Bioengineering, and [2]Electrical and Computer Engineering,

Rice University, 6100 Main Street, Houston, TX 77005, USA

* Email: drezek@rice.edu

(713) 348-3011 (office)

Abstract

We have developed a miniaturized high-resolution low-cost reflectance-mode fiber microscope (RFM) aimed at optical tissue biopsy applications using a polarized imaging configuration to suppress background noise from specular reflectance. The RFM is equipped with an air-cooled light-emitting diode illumination module and a single 450-µm outer-diameter fiber bundle image guide compatible with a 20-gauge needle. The dual illumination and image acquisition nature of the fiber bundle simplifies the system and reduces the total cost. Imaging tests with a US Air Force resolution target demonstrate a lateral resolution of ~3.5 µm. The performance of the imaging system was evaluated examining samples of cells and excised human tissue. Still and video rate images are obtainable in reflectance mode using intrinsic contrast.

Standard pathology requires removal of cells or tissue through techniques ranging from fine needle aspiration or core needle biopsy to surgical resection. To allow examination of suspect lesions, a variety of endoscopic imaging techniques may be employed including fiber-scanning confocal microscopy in reflectance [1-3] and fluorescence [4, 5] modes. These techniques use an optical fiber or fiber bundle to view the surface of interior body cavities. Images are created by scanning mechanisms positioned at either the distal or proximal ends of the fiber. These types of systems can capture point by point high resolution images from a large field of view, and the sensitivity of the systems can be very high [6-8]. Recent advances provide similar high resolutions images using simple, low-cost systems based on coherent fiber bundles with images captured using inexpensive digital cameras [9-11]. Image resolution is limited by the individual fibers of the fiber bundle. A fluorescent-mode fiber endoscope developed by Muldoon *et al*. achieves a resolution of ~4.4 μm [9, 10]. We are developing a high-resolution (~3.5 μm) reflectance-mode endoscope that is flexible, compatible with a 20-gauge needle, and can generate still and video rate images using intrinsic contrast. Reflectance-mode endoscopic imaging can potentially complement fluorescence imaging by capturing information not available in fluorescence mode and by functioning in situations when fluorescent imaging is not practical.

In this article, we present a needle-based, high-resolution reflectance-fiber microscope (RFM) developed for optical tissue biopsy applications. The RFM was assembled on a portable $18 \times 24 \times 1/2$ inch^3 aluminum breadboard to facilitate eventual clinical trials. As shown in Fig. 1, an air-cooled light-emitting diode (Luxeon; white LED, model LXHL-NWE8; blue LED, model LXHL-NRR8) served as the illumination source

to keep the RFM as compact as possible and reduce the system cost. The light from the LED is collimated by an integrated collimating lens and passes through a linear polarizer (Fig. 1), after which the polarized light is reflected by a glass slide positioned at ~45° (with respect to the beam trajectory) and projected onto an infinity-corrected 10× objective lens (Newport, model: L-10x, 0.25NA). The objective lens and a fiber chuck (Newport, model: FPH-DJ) are positioned with a multimode fiber-coupler positioner (Newport, model: F-915T). By careful alignment, the illumination light is focused into the incident end of a 450-μm outer-diameter fiber image guide which is positioned by the fiber chuck (Sumitomo Electric, model: IGN-037/10, 10^4 fiber elements in a picture area of 333 μm diameter, 0.35NA) [12]. Finally, the imaging end of the fiber image guide is inserted into the core of a 20-gauge needle and positioned in contact with the samples. Light scattered from the samples is collected by the same illumination fiber and passes back through the same 10× objective lens and glass slide described previously (see Fig. 1).

A CCD color camera (Edmund Optics, model: EO-0813C) coupled with a circular polarizer filter (Nikon, 62mm) is used to sample the fiber bundle elements for image acquisition. Because the polarization orientation of the S-polarized illumination light is perpendicular to the plane of incidence with respect to the glass slide (i.e., the plane of the Fig. 1), a significant portion is reflected toward the incident end of the fiber bundle to be delivered to the imaging end of the fiber bundle. Specular reflectance from the incident end of fiber bundle is also partly reflected away by the glass slide, and the remaining specular reflectance is further suppressed by the circular polarizer in front of the CCD camera that passes P-polarized light with respect to the plane of incidence. Rays

that result from multiple scattering events changing their polarization to the parallel direction can be detected by the CCD camera (e.g., light scattered from the sample). Thus, noise from specular reflection from the incident end of the fiber bundle is greatly suppressed, and clearer images are collected.

Figure 2(a) shows a reflectance image of the fiber bundle imaging end when the needle microscope is positioned in air. Light from the white LED that is reflected from the glass-air interface at the imaging end of the fiber bundle is successfully detected by the CCD camera, and individual fibers of the fiber bundle are resolved (Fig. 2a). With the imaging needle of the RFM immersed into a vial of water or phosphate-buffered saline (PBS) solution, the RFM field of view is almost completely dark because the close match between the refractive indices of water and the glass fiber result in dramatically reduced internal reflection from the imaging end of the fiber bundle.

Figure 2(b) is obtained with a drop of water covering the tip of the imaging fiber bundle, which mimics the immersion of fiber tip in water, to provide clear image features. Much less internal reflection occurs from the imaging area covered by water [Fig. 2(b)] compared with the same area when it is exposed to air. Figures 2(a) and (b) were captured with the same imaging configurations and the index-matching effect is clear. When used in biological or clinical environments, the fiber bundle tip is always in contact with body fluids or tissue. Thus, dipping the fiber-bundle tip into water roughly approximates the conditions of realistic imaging application. In liquid, the reduced internal reflectance leads to a dark field-of-view and a decrease in background enabling biological imaging. Light scattered by biological structures can be clearly distinguished and cellular images can be obtained. In contrast to the polarized reflectance-mode images

in Figures 2(a) and (b), images shown in Figs. 2(c) and (d) were captured with a reduced exposure time under the same imaging conditions but without the illumination and collection polarizers. The specular-reflectance from the optical components makes it impossible to obtain useful information from Figs. 2(c) and (d).

A white LED was used to acquire the images and plots shown in Figs. 3(a) to (c) and Video 1. Figure 3(a) shows an imaging resolution of ~3.5 µm (~143 line pairs/mm) obtained upon imaging the US Air Force resolution target. Figure 3(b) shows that contrast decreases slightly from low (64lp/mm) to high (128lp/mm) resolution, but it also reveals high frequency components due to the probe fibers (3.3 µm dia.). Figure 3(c) and Video 1 were obtained by using the same white LED-illuminated RFM to image skin tissue from a green onion. The cell walls of the rectangular green onion skin cells [13] are clearly resolved in both the still image and the video. Note that water was used in all the tests to provide refractive index matching.

The LED light source is cost-effective and easy to change. An air-cooled blue LED was used to image cultured SKBR3 human carcinoma cells. Before imaging, SKBR3 carcinoma cells were cultured in a 6 mm plate at 37 °C for 2 days. The fiber bundle tip was immersed into the culture medium through a needle and focused onto a group of cells attached to the culture plate. As shown in Fig. 3(d), the cells can be visualized with the RFM using blue-LED illumination. An endoscopic video clip of the SKBR3 cancer cells is provided in Video 2. The same RFM was also used to image excised human oral cancer tissue obtained from the Cooperative Human Tissue Network (CHTN). The tissue was placed in a culture plate with PBS which was then placed on a two-dimensional translation stage. The needle and fiber-bundle tip were inserted into the

tissue sample and cellular structures were visualized as shown in Figure 4 and Video 3. In Video 3, cellular images move in and out of focus as the imaging tip moves closer to or further away from the sample. The same RFM was used to image the reflectance from a dust particle in liquid solution to demonstrate single pixel fiber resolution as shown in Video 4.

In this letter, we have described a high-resolution RFM developed for optical tissue biopsy applications. The resolution of this fiber microscope is limited by the element fiber size of the imaging fiber bundle. For the specific fiber-bundle image guide presented in this letter, the resolution is ~3.5 µm. The reported RFM system uses the same fiber-bundle guide for both illumination and imaging. A pair of cross-polarized filters is used in addition to the fiber-bundle guide to achieve high-resolution reflectance-mode microscopic imaging. The fiber-bundle guide is 450 µm in diameter, making it compatible with current clinical needle tissue biopsy systems. The RFM system can be used without external agents when there is sufficient endogenous imaging contrast. Moreover, with simple filter changes, the RFM system can readily be converted to a fluorescence-mode needle-biopsy imaging system similar to that developed Muldoon *et al* [9]. Future work will assess whether performance can be improved through the use of simple chemical agents already in routine clinical use.

Acknowledgments

References

1. C. Liang, M. Descour, K. B. Sun, and R. Richards-Kortum, "Fiber confocal reflectance microscope (FCRM) for in-vivo imaging," *Opt. Express* **9**, 821-830 (2001).

2. S. Yoshida, S. Tanaka, M. Hirata, R. Mouri, I. Kaneko, S. Oka, M. Yoshihara, and K. Chayama, "Optical biopsy of GI lesions by reflectance-type laser-scanning confocal microscopy," *Gastrointest Endosc* **66**, 144-149 (2007).

3. K. C. Maitland, A. M. Gillenwater, M. D. Williams, A. K. El-Naggar, M. R. Descour, and R. R. Richards-Kortum, "In vivo imaging of oral neoplasia using a miniaturized fiber optic confocal reflectance microscope," *Oral Oncol.* **44**, 1059-1066 (2008).

4. A. F. Gmitro, and D. J. Aziz, "Confocal microscopy through a fiber-optic imaging bundle," *Opt. Lett.* **18**, 565-567 (1993).

5. F. Jean, G. Bourg-Heckly, and B. Viellerobe, "Fibered confocal spectroscopy and multicolor imaging system for in vivo fluorescence analysis," *Opt. Express* **15**, 4008-4017 (2007).

6. R. Juskaitis, T. Wilson, and T. F. Watson, "Real-time white light reflection confocal microscopy using a fiber-optic bundle," *Scanning* **19**, 15-19 (1997).

7. V. Dubaj, A. Mazzolini, A. Wood, and M. Harris, "Optic fiber bundle contact imaging probe employing a laser scanning confocal microscope," *J. Microsc.* **207,** 108-117 (2002).

8. R. Kiesslich, M. Goetz, M. Vieth, P. R. Galle, and M. F. Neurath, "Technology Insight: confocal laser endoscopy for in vivo diagnosis of colorectal cancer" *Nat Clin Pract Oncol* **4**, 480-490 (2007).

9. T. J. Muldoon, M. C. Pierce, D. L. Nida, M. D. Williams, A. Gillenwater, and R. Richards-Kortum, "Subcellular-resolution molecular imaging within living tissue by fiber microendoscopy," *Opt. Express* **15**, 16413-16423 (2007).

10. T. J. Muldoon, S. Anandasabapathy, D. Maru, and R. Richards-Kortum, "High-resolution imaging in Barrett's esophagus: a novel, low-cost endoscopic microscope," *Gastrointestinal Endoscopy* **68**, 737-744 (2008).

11. T. J. Muldoon, N. Thekkek, D. Roblyer, D. Maru, N. Harpaz, J. Potack, S. Anandasabapathy, and R. Richards-Kortum, "Evaluation of quantitative image analysis criteria for the high-resolution microendoscopic detection of neoplasia in Barrett's esophagus," *J. Biomed. Opt.* **15**, 026027 (2010).

12. Sumitomo Electric. "Silica image guide for fiberscope," Proprietary Technical Document (2008).

13. A. G. von Arnim, X. W. Deng, and M. G. Stacey, "Cloning vectors for the expression of green fluorescent protein fusion proteins in transgenic plants," *Gene* **221**, 35-43 (1998).

Figure 1: Schematic of the reflectance fiber imaging system.

Figure 2: Reflectance images of the fiber-bundle tip glass/air interface showing greatly reduced specular background using this RFM system in comparison with the non-polarized imaging system. The images (a) and (b) were obtained using cross-polarized illumination and imaging filters. For image (a), the fiber tip was in air. For image (b) fiber tip was covered with a drop of water. Images (c) and (d) were obtained without polarized illumination and imaging filters. Image (c) is with the fiber tip in air, whereas image (d) is with the fiber tip covered with a drop of water.

Figure 3: Processed endoscopic images of (a) USAF resolution target showing the resolution of ~143lp/mm, acquired with white LED illumination, (b) cross sections of two resolution line-pair sets showing both the line-pair intensity variation and variation due to probe fibers (3.3μm dia.), (c) onion skin cells (see also Video 1), where arrows show the resolved cell walls, acquired with white LED illumination, and (d) cultured SKBR3 cancer cells (see also Video 2), where the arrows indicate resolved single cells, acquired with blue LED illumination. Scale bar: 50 μm.

Figure 4: Endoscopic images of excised oral cancer tissue including (a) processed image showing cellular structures (see also Video 3) and (b) processed images with drawn lines superimposed to indicate the estimated cell boundaries. Scale bar is 50 μm.

Video 1: Reflectance endoscopic video of onion skin cells showing the resolved cell walls.

Video 2: Reflectance endoscopic video of cultured SKBR3 cells.

Video 3: Reflectance endoscopic video of a sample of excised human oral cancer tissue showing the resolved cellular structures. In this video, cellular images move in and out of focus as the imaging tip moves closer to or further away from the sample.

Video 4: Reflectance endoscopic video of a dust particle in liquid solution showing single pixel fiber resolution.

LED

Collimation lens

S-polarization filter

Image guide

CCD

Needle

P-polarization filter

Glass slide

Objective

Sample

Distance from lp edge, 128lp/mm [μm]

Distance from lp edge, 64lp/mm [μm]